Deep Learning Driven Simulations of Boundary Layer Clouds over the ~~US~~

Southern Great Plains

Tianning Su[1]*, Yunyan Zhang[1]

[1]Lawrence Livermore National Laboratory, Livermore, CA, USA

Submission to *Geoscientific Model Development*

*Corresponding authors: *su10@llnl.gov*

Abstract. ~~This study developed~~ Based on long-term observations at the Southern Great Plains site by the Atmospheric Radiation Measurement (ARM) program for training and validation, a deep learning model is developed to simulate the ~~complex dynamics~~daytime evolution of boundary-layer clouds (BLCs) ~~over the US Southern Great Plains. Using over twenty years of extensive observations from the Atmospheric Radiation Measurement program for training and validation, the model diagnoses the BLCs~~ from the perspective of ~~cloud~~-land-atmosphere coupling. ~~Morning~~The model takes ARM measurements as inputs including early-morning soundings and the diurnal-varying surface meteorological ~~profiles set as the initial~~ conditions and ~~then identifying triggers for BLCs formation from surface meteorology.~~heat fluxes and predicts hourly estimates as outputs including the determination of cloud occurrence, the positions of cloud boundaries, and the vertical profile of cloud fraction. The deep learning model ~~offer accurate simulation of the convection initiation and cloud base of BLCs. In comparison~~offers a good agreement with the observed cloud fields, especially on the accuracy in reproducing cloud occurrence and base height. If substituting the inputs by reanalysis data ~~(i.e.,~~from ERA-5 and MERRA-2~~), it provides a notable improvement in the vertical structure,~~ the outputs of ~~low clouds from a climatological perspective. The~~ the deep learning model ~~can~~ provide a better agreement with observation than the cloud fields extracted from ERA-5 and MERRA-2 themselves. From such practice, the deep learning model shows great potential to serve as ~~the cloud parameterization and extend to analyzing~~a diagnostic tool on the performance of physics-based model~~s performance~~ in simulating stratiform and cumulus clouds ~~within reanalysis frameworks, offering~~.

45   By quantifying biases in clouds and attributing them to the simulated atmospheric state

46   variables versus the model parameterized cloud processes, this observation-based deep

47   learning model may offer insights ~~into improving~~on the directions to improve the

48   simulation of BLCs~~. By quantifying biases due to various meteorological factors and~~

49   ~~parameterizations, this deep learning-driven approach bridges the observational-~~

50   ~~modeling divide. Surface humidity and parameterization emerge as key limiting factors~~

51   ~~to affect the representation of BLCs in the reanalysis data. This deep learning approach~~

52   ~~holds promise for improving the convection parameterization and advancing model~~

53   ~~diagnostics in~~ in physics-based models for weather forecasting and climate

54   ~~modelling~~ prediction.

1 Introduction

Boundary layer clouds (BLCs), comprising primarily of ~~stratiforms~~stratiform and shallow cumuli, exert a profound influence on the Earth's radiative balance ~~and climate system~~ (Betts, 2009; Teixeira and Hogan, 2002; Lu et al., 2013; Golaz et al., 2002). Their formation and evolution ~~within the planetary boundary layer (PBL)~~ are critically shaped by the interactions between surface ~~processes~~, planetary boundary layer ~~the~~ (PBL) and ~~atmospheric dynamics~~free troposphere (Miao et al., 2019; Berg and Kassianov, 2008; Zhang and Klein, 2013; Guo et al., 2019; Zhang et al., 2017). ~~These clouds, which frequently form in the PBL's entrainment zone, are the critical part for weather prediction and climate modeling, holding the key to understanding land-atmosphere interactions (Caldwell et al., 2021; Bretherton et al., 2007; Wang et al., 2020, 2023; Moeng et al., 1996; Su et al. 2023; Zhang and Klein, 2010; Guo et al., 2019).~~

Numerous studies ~~have been dedicated to~~ investigat~~ing~~ed the ~~dynamics~~controlling factors of ~~boundary layer clouds~~BLCs, highlighting the pivotal role of the land surface in modulating cloud formation and affecting the spatial and temporal distribution of low clouds (Zhang and Klein, 2010; 2013; Rieck et al., 2014; Xiao et al., 2018; Lareau et al., 2018; Lee et al., 2019; ~~Fast et al., 2019b; Tang et al., 2018;~~ Tang et al., 2019; Tao et al., 2019; Tian et al., 2022~~; Qian et al., 2023). Despite considerable advancements~~).

These clouds, which frequently form in ~~observations and~~ the PBL's entrainment zone, are very challenging to be simulated in weather prediction and climate modeling ~~capabilities, simulating the boundary layer clouds remains a significant challenge, largely~~ due to the small scales of their operating physics and the complex feedback

mechanisms between land surface fluxes, PBL turbulent processes, and cloud microphysics (Miao et al., 2019; Lareau et al., 2018; Lu et al., 2011; Fast et al., 2019a; Wang2019; Morrison et al., 2014. 2020; Yang et al., 2018; Nogherotto et al., 20162016; Caldwell et al., 2021; Wang et al., 2023; Guo et al., 2019). These challenges are compounded when attempting to represent such processes in global and regional climate models, where the fine-scale interactions are often parameterized in a coarse-resolution grid due to computational constraints (Bretherton et al., 2007; Moeng et al., 1996). In addition, different cloud regimes exhibit variedcomplex nonlinear cloud-land interactions that complicate their representation and present, which pose challenges for observational studies and modeling efforts, particularly for physicalempirical parameterizations (Tang et al., 2018; Qian et al., 2023; Sakaguchi et al., 2022; Poll et al., 2022; Tao et al., 2021).

As an emerging tool, machine learning (ML) has been widely employed for a variety of environmental and atmospheric studies (e.g., McGovern et al., 2017; Gagne et al., 2019; Vassallo et al., 2020; Cadeddu et al., 2009; Molero et al., 2022; Guo et al., 2024). Specifically, ML techniques are increasingly being employed to simulate and estimate convection and precipitation, which are crucial for accurate weather forecasting and climate modeling (Mooers et al., 2021; Wang et al., 2020; O'Gorman et al., 2018; Gentine et al., 2018; Zhang et al., 2021). For example, Rasp (2020) presents algorithms for the implementation of coupled learning in cloud-resolving models and the super parameterization framework. Similarly, ML tools have been applied to leverage observational data for the refinement of convection parameterizations, offering

more insights into convective triggering (Zhang et al., 2021). ~~dynamics~~In addition, ML has been used to emulate convection schemes and develop parameterizations using data from advanced simulations (O'Gorman ~~et al.,~~and Dwyer, 2018; Gentine et al., 2018~~;~~). Furthermore~~Zhang et al., 2021). Moreover~~, Haynes et al. (2022) develop pixel-based ML-based methods of detecting low clouds, with a focus on improving detection in multilayer cloud situations and specific attention given to improving ~~the~~ cloud characteristics~~zation~~.

. Despite the considerable advancements brought by ML, there are persistent challenges in accurately simulating the vertical structure of clouds, as well as their complex relationships with land surface. ~~To address these complexities, this study developed an advanced deep-learning framework to simulate the BLCs, using comprehensive data from the Atmospheric Radiation Measurement (ARM) program at the Southern Great Plains (SGP) site. This framework is designed to simulate the triggers, progression, and structural structure of boundary layer clouds, placing a particular emphasis on cloud-land coupling mechanisms. By assimilating morning radiosonde observations with diurnal-varying surface fluxes and meteorological data, this deep learning model is uniquely positioned to unravel the complex initiation and evolution of low clouds, especially those coupled with land surface processes..~~

Southern Great Plains (SGP) site, as part of the U.S. Department of Energy Atmospheric Radiation Measurement (ARM) program, is crucial for cloud evaluation and climatology studies in modeling efforts. Recognized globally as a leading climate research facility, the ARM SGP site (36.607°N, 97.488°W) has been collecting a wealth

of meteorological and radiative measurements, offering data that spans over two decades (Sisterson et al. 2016). The rich dataset from the ARM SGP site can help address persistent challenges in cloud modeling. This study leverages these extensive observations to build a deep learning model, serving as an observation-based "emulator" for simulating BLCs. Our model enhances the estimations for cloud fields of BLCs, particularly cloud occurrence, position, and fraction. Furthermore, the critical assessment of our model in comparison with existing reanalysis datasets, including MERRA-2 and ERA-5, highlights the improvement in ~~representing~~estimating cloud vertical structure. Our study analyzed the model's performance across ~~various~~different cloud regimes, such as stratiform and cumulus. ~~By serving as the cloud parameterization in the reanalysis data, this model advanced the capability of low cloud simulations within reanalysis frameworks.~~ By undertaking this endeavor, we ~~strive~~aim to ~~narrow~~help bridge the existing gaps ~~in boundary layer clouds~~representing BLCs between field observations and modeling by a deep learning model of BLCs, thereby improving diagnostics of model performance and enriching our understanding of the BLC~~convective~~ processes.

2 Data ~~and instruments~~Description

2.1 ~~Comprehensive observations at~~Observations for the ~~US Southern Great Plains~~

~~The ARM program, funded by~~ development of the ~~U.S. Department of Energy, plays a pivotal role at the SGP site in Oklahoma (36.607°N, 97.488°W). Recognized globally as a leading climate research facility, the ARM SGP site has been collecting a wealth of meteorological and radiative measurements, offering data that spans over two decades.~~ deep learning model

This study utilized ~~these extensive field~~ the ARM SGP observations during 1998-2020 to ~~explore~~ serve as training, validation, and testing data for the development of the ~~simultions~~deep learning model. Note that all the observations are collected at the central facility of ~~BLCs from the deep learning techniques.~~

~~Our study employs the Active Remote Sensing of Clouds (ARSCL) product~~SGP, a fixed location, which ~~integrates lidars, ceilometer,~~is different from other ML studies that use global data from reanalysis or climate model simulations (e.g., O'Gorman and ~~cloud radar~~Dwyer, 2018; Shamekh et al. 2023).

The input data to ~~define cloud boundaries, utilizing~~train and validate the ~~best estimates from lidar for the lowest cloud bases (Clothiaux et al. 2000, 2001; Kollias et al. 2020). Based on the comprehensive information of cloud vertical structure and temporal evolution from the ARSCL dataset, Xie et al. (2010) offers detailed cloud fraction profiles at the hourly resolution in ARM BEST ESTIMATE DATA PRODUCTS (ARMBE).~~

160 ~~Central to our analysis are the comprehensive thermodynamic profiles obtained~~

161 ~~from~~ deep learning model include early morning sounding data and diurnal varying

162 surface meteorological conditions and surface turbulent heat fluxes. We take

163 radiosondes (SONDE~~). Launched routinely at multiple times daily, these SONDE~~)

164 measurements around 6 a.m. local time to offer ~~detailed information into the~~

165 thermodynamic ~~state of~~and wind profiles in the PBL and the free atmosphere. ~~The~~

166 ~~operation and technical aspects of the ARM SONDE are detailed in~~ (Holdridge et al.

167 (2011~~).~~

168) as initial conditions. SONDE launches typically took place four times per day at

169 the SGP site, usually at 00, 06, 12, and 18 local times. Local time, defined as daylight

170 saving time, is used consistently throughout the year. Each morning profile comprises

171 46 levels spanning from 0-8 km, which include levels at intervals of 50 meters from 0

172 to 1 km, 0.1 km from 1 to 2 km, 0.25 km from 2 to 4 km, and 0.5 km from 4.5 to 8 km.

173 Meanwhile, ~~We use~~ the collocated surface meteorology systems (MET, Ritsche, 2011)

174 provide a variety of meteorological ~~parameters~~measurements (i.e., temperature, relative

175 humidity, wind, and pressure) at the surface ~~level from collocated surface meteorology~~

176 ~~systems (MET) at the ARM SGP site. These surface meteorological parameters play~~

177 ~~roles in the formation and development of BLCs. Furthermore, the site also provides~~

178 ~~data on surface~~. Surface sensible and latent heat fluxes. ~~An~~ are taken from the ARM

179 value-added product called the best-estimate fluxes from ~~energy balance Bowen ratio~~

180 ~~measurements and~~the Bulk Aerodynamic calculations of the Energy Balance Bowen

181 ratio measurements (BAEBBR~~), was generated to replace the energy balance Bowen~~

182 ~~ratio flux measurements with a bulk aerodynamic estimation when the Bowen Ratio~~

183 ~~has a range of −1.6 and −0.45 (,~~ Cook, 2018). ~~The replacements generally happen for~~

184 ~~the measurements at a 30-min temporal resolution under the low sensible heat scenario.~~

185 ~~We use the BAEBBR data along with~~

186   In addition, we also use derived variables based on observations as the input fields

187 into the deep learning model. LCL is derived from the surface meteorology (Romps,

188 2017), BLH_{parcel} (boundary layer height derived from parcel methods) is calculated

189 from the morning temperature profiles and surface air temperature (Holzworth, 1964;

190 Su and Zhang, 2024). Specifically, BLH_{parcel} is defined as the height where the morning

191 potential temperature profile first exceeds the current surface potential temperature by

192 more than 1.5 K. Meanwhile, BLH_{SH} (boundary layer height derived from sensible heat

193 flux) is calculated from the morning temperature profiles and surface sensible heat

194 (Stull, 1988; Su et al. 2023).

195   For the target data of model outputs to train and validate the deep learning model,

196 our study employs hourly cloud fraction data available from the ARM Best Estimate

197 (ARMBE, Xie et al, 2010) dataset. This cloud fraction is developed based on the Active

198 Remote Sensing of Clouds (ARSCL, Clothiaux et al. 2000, 2001; Kollias et al. 2020),

199 which utilizes the best estimates from ceilometer for the lowest cloud bases and

200 integrates micro-pulse lidar, ceilometer, and cloud radar data to define cloud tops and

201 cloud fraction. In addition, to construct learning targets, the base of BLC is determined

202 at the lowest altitude where the cloud fraction first exceeds 1%, and the cloud top is

203 identified at the point where the cloud fraction transitions from exceeding 1% to falling

below this threshold. In multi-layer systems, the DNN model is trained based on the lowest cloud layer when it is coupled with the land surface. However, we do not exclude multiple-layer cloudy cases if their vertical fractions are continuous from the lower to upper layer. as the key input for the deep learning model.

Based on ARM observations, this study developsed an advanced deep-learning framework to simulate the BLCs, using detailed observational data, including SONDE profiles, surface meteorological measurements, and ARSCL, from the SGP site. This framework is designed for BLCs, placing a particular emphasis on cloud-land coupling mechanisms. By integrating morning SONDE observations with diurnally varying surface fluxes and meteorological data, this deep learning model is capable of diagnosing the initiation and evolution of low clouds, especially those coupled with land surface processes. By serving as an offline diagnostic tool, this model aims to enhance low cloud simulations within reanalysis frameworks without being embedded in the simulations that produce the reanalysis data itself.

2.2 Classification of coupled bBoundary layer clouds from oObservations

The deep learning model in this study aims to simulate BLCs demonstrate complex evolutions and interactstrongly coupled with boundary layer and land surface processes. TrackingThe classification of clouds below is to filter the initiation, development, and lifecycle of BLCs is crucial for understandingbased on the convection in our climate

226 system. Weconcept of cloud-land coupling and is important for the training and analysis

227 of the deep learning model. Here, we treat BLCs as synonymous with land-coupled

228 clouds, in contrast to those clouds that are decoupled from the PBL and land surface.

229 In this regard, Su et al. (2022) devised a lidar-based method to discern cloud-land

230 coupling, leveraging the vertical coherence and temporal continuity of the PBL. This

231 approach, combined with cloud base height measurements from ceilometers and

232 surface-based Lifting Condensation Level (LCL) calculations as proposed by Romps

233 (2017), forms the foundation for identifying coupled low-level clouds in our study. The

234 methodology for determining PBLH, as outlined by Su et al. (2020), established a long-

235 term record of PBLH at the SGP. The resulting data are publicly available through the

236 ARM database (https://www.arm.gov/data/data-sources/pblht-206).

237   Coupled clouds are identified when the cloud base height (CBH), as derived from

238 the ceilometer, aligns with or is below the lidar-detected PBL top height within 0.2 km,

239 and the calculated surface-based Lifting Condensation Level (LCL, Romps 2017) falls

240 within a certainmaximum allowable range of 0.7 km (Su et al. 2022).2022). PBL height

241 data (https://doi.org/10.5439/2007149, Su et al. 2020) are publicly available through the

242 ARM database. This alignment is indicative of clouds that are directly influenced by

243 surface-driven processes. Meanwhile, we apply a cloud thickness threshold of less

244 than(< 4 km) is applied to analyze ensure the occurrence of BLCs. (i.e., not deep

245 convective clouds).

246   Within the scope of land-coupled clouds, we further classify the observed daytime

247 BLCs into cumulus and stratiform categories. following the methodology in Su et al.

(2024). Stratiform cloud days are identified by prolonged overcasting conditions during the daytime, lasting more than three hours, with the maximum cloud fraction exceeding 90% based on ARSCL data. For cumulus ~~clouds~~cloud days, two criteria are applied: (1) cloud formations emerge after sunrise, ensuring that they are driven by local convective processes, and (2) there is an absence of ~~overcasting clouds. Conversely, stratiform clouds are identified by prolonged overcasting conditions during the daytime, typically lasting more than three hours, with cloud fractions exceeding 90% as per ARSCL data.~~ ~~Based on the~~stratiform clouds. Based on these criteria, we identified 940 days categorized under the cumulus regime, distributed as 21%, 56%, 17%, and 6% across Spring, Summer, Fall, and Winter, respectively. Similarly, we identified 657 days falling within the stratiform clouds regime, with respective seasonal distributions of 37%, 12%, 23%, and 28%. ~~This classification of cloud types to filter the BLCs based on the concept of cloud-land coupling is important for the training and analysis of the deep learning model. We further attempt to use the comprehensive cloud observations at the SGP to build the deep learning model.~~Note that this cloud regime classification is done on a daily basis. To maintain clarity in our analysis, we excluded days with mixed cloud regimes, focusing only on days that exhibit only stratiform or cumulus clouds during the daytime.

2.3 Reanalysis data for the application of the deep learning model

~~In this study, we also use~~To demonstrate how to use the deep learning model, we take advantage of reanalysis datasets from the European Centre for Medium-Range

Weather Forecasts' fifth-generation global reanalysis (ERA-5, Hersbach et al., 2020) and NASA's Modern-Era Retrospective analysis for Research and Applications Version 2 (MERRA-2, Gelaro et al., 2017).2017). Note that unlike observational data aforementioned, reanalysis data are not used for training the deep learning model, instead they are going to be used to help illustrate how the deep learning model may disentangle the potential causes leading to the biased cloud simulations.

As the state-of-art reanalysis data, the ERA-5 is producedprovides hourly atmospheric states and cloud fraction around SGP by the Integrated Forecasting System (IFS) and a data assimilation system at a fine spatialhorizontal resolution of 0.25° x 0.25°. ERA-5 reanalysis data are obtained from the Copernicus Climate Data Store. This dataset° and a vertical resolution of 25 hPa in the lower atmosphere (700 – 1000 hPa). IFS employs a prognostic cloud scheme capable of capturing the evolution of cloud dynamics over consecutive time steps (Tiedtke 1993), a feature that enhances its utility in time-dependent climate studies. We also use ERA-5 data to obtain the cloud and atmospheric information, which provides the hourly measurements at a 0.25° – 0.25° longitude-latitude grid. The vertical resolution of ERA-5 data is 25 hPa in the lower atmosphere (700 – 1000 hPa).

The MERRA-2 reanalysis data use a new version of the provides hourly low cloud fraction and 3-hourly vertical cloud fraction profiles at a spatial resolution of 2/3° (longitude) × 1/2° (latitude). MERRA-2 is based on the Goddard Earth Observing System Data Assimilation System Version 5, which is a advanced system coupling a global atmospheric general circulation model to NCEP's Grid-point Statistical

Interpolation analysis (Randles et al., 2017). The MERRA-2 reanalysis has a spatial resolution of 2 / 3° × 1/2° (longitude = latitude). MERRA-2 and utilizes a diagnostic cloud scheme, focusing on the immediate state of clouds (Randles et al., 2017). This dataset specializes in the representation of the hydrological cycle and cloud information, which are widely used in multiple studies (e.g., Yeo et al., 2022; Kuma, 2020; Miao et al., 2019). MERRA-2's reanalysis provides detailed hourly low cloud fraction data and tri-hourly vertical cloud fraction profiles.

Here we acknowledge the local heterogeneity of cloud fields in the area covered by an ERA5 or MERRA grid cell. This inherent discrepancy between the reanalysis data and the ARM SGP observations may arise from the difference between point-based measurements and area-based assimilated grid-averages. However, observations at the SGP site, representative of plain regions, have been widely used for evaluating models across scales from climatological and statical perspectives (e.g., Song et al., 2014; Zhao et al., 2017; Zheng et al., 2023; Zhang et al., 2017).

3 Construction of the Deep Learning FrameworkModel for Simulating Boundary Layer Clouds

3.1 Integrated Deep Learning Models for Cloud Simulation

3.1 Structure design of the deep learning model

This study developeddevelops an integrated deep learning approachmodel to simulate BLC over the SGP site. These models are, whose design is illustrated in Figure

1. Traditionally, simulating BLCs involves solving complex equations related to PBL turbulence and cloud microphysical processes. Our approach, however, leverages deep learning to bypass these intricate simulations. By using module-specific hidden layers, the deep learning model serves as an observation-based "emulator" that directly estimates BLCs from early-morning soundings and surface-related parameters.

The model is purpose-built to ~~simulate the initiation, positioning, and vertical extent of BLCs. Figure 1 demonstrates the design of our deep learning framework. The core~~consist of ~~this research integrates~~ three distinct deep learning ~~models~~modules, each responsible for a critical aspect of the cloud simulation: ~~the triggering of cloud formation,~~1) the determination of ~~cloud~~ the BLC occurrence, 2) the height position~~,~~ ~~and the vertical profile~~ of the cloud base, and 3) the cloud thickness and the normalized 10-layered shape of ~~coverage~~cloud fraction within cloud boundaries, which jointly ~~yielding the comprehensive features~~yield the hourly-averaged vertical structures of BLCs ~~through~~. This modular approach ensures that the estimations are specific for each aspect of the BLCs. Combining cloud thickness and cloud fraction in one module is logical because the thickness for 10-layered clouds varies based on cloud thickness, and thickness is potentially related to the fraction, as thicker clouds are sometimes associated with larger cloud fractions. Naturally, cloud top is considered as the cloud base plus the thickness. This separation of tasks enhances the overall reliability and clarity of the model in capturing the various characteristics of BLCs. Note that each of the three deep learning modules is built upon a deep neural network (DNN) with multiple hidden layers. ~~Initially,~~

The occurrence module, as the ~~triggering model~~first step, evaluates ~~whether~~the likelihood of cloud formation ~~is likely,~~by producing a ~~value~~number between 0 and 1, ~~with values~~ which we call "trigger" in the following, whose value above 0.5 ~~indicating~~indicates the presence of clouds. ~~This triggering~~The target data for this module is binary (0 or 1), and the model output is a continuous value between 0 and 1. This occurrence information then feeds into the other two ~~models~~modules in parallel: one for ~~determining the cloud's position~~locating cloud boundaries and the other for ~~calculating~~delineating the vertical shape of the cloud fraction in cloudy layers. While the cloud ~~position~~base (or boundary) module and ~~cloud~~the fraction ~~models~~thickness (or fraction) module are independent ~~components~~of each other, they collaborate to depict the vertical cloud fraction profile.

~~Morning meteorological profiles set as the initial conditions and then identifying triggers for BLC formation from surface meteorology. Each morning profiles have 46 elements from 0-6km. For surface meteorology and fluxes, the inputs include the data at the current hour and the previous hour. The RH profiles and PBL top are highlighted for their significance in boundary layer development.~~ To represent the vertical structure of BLC~~, we equally~~ in the fraction-thickness module, we segmented the cloud layer from the base to the top into ten levels.~~ For each of these levels, our deep learning models calculate individual cloud fraction values~~, with each level's thickness varying according to the overall cloud thickness. These values are then interpolated to create a continuous vertical profile of cloud fraction within the BLC~~, offering a detailed depiction of the cloud's vertical extent. This model used~~ boundaries, offering a detailed

358 depiction of the cloud's vertical extent. The vertical position of the layer changes based

359 on the predicted cloud base and top to accurately represent the vertical structure of

360 BLCs. This dynamic approach allows the fraction module to adjust and focus on the

361 relevant portions of cloud fraction within cloudy layers. Compared to a static height-

362 level approach, which requires the prediction of cloud fraction across a fixed vertical

363 extent (e.g., multiple levels between 0-6 km), our method focuses on the shape of the

364 fraction profile. This ensures the model is not constrained by fixed vertical levels,

365 allowing for more efficient and robust estimations.

366

367 **3.2 Deep Neural Network (DNN) architecture and configuration**

368 The construction of the deep learning model uses the TensorFlow Package,

369 developed by Google (https://www.tensorflow.org/). Each module in the deep learning

370 model is constructed based on a separate deep neural network (DNN) respectively. The

371 DNN architecture is designed, beginning with an input layer reflective of the selected

372 feature set, which includes morning sounding profiles, surface meteorology and heat

373 fluxes data, and the derived variables such as LCL, BLH_{parcel} and BLH_{SH}. For predicting

374 the current hour BLC, the inputs of surface conditions include data both at the current

375 hour and the previous hour. The input variables for training and validating the deep

376 learning model are detailed in Table 1, including variable names, descriptions, and data

377 sources, together with the ARMBE cloud fraction profiles as the learning target for

378 model outputs.

The deep neural network (DNN) architecture was designed (brown boxes in Figure 1), beginning with an input layer reflective of the selected feature set. The detailed structures for the three models can be found in Table 1. Normalization is, a preprocessing technique that often leads to improvements in model training by scaling the input features and target values to a standard range (Raju et al. 2020). We , was applied the normalization process to both the input and target data to ensure that they havescale them to a zero mean and a standard deviation of one (Klambauer et al. 2017; Salimans and Kingma, 2016; Raju et al. 2020). This standardization scalesensures that the data is scaled to a common range, allowing for a more stable and efficientoffers some benefits, such as improving the stability and efficiency of the training process. Subsequent

The architecture of the DNN models was structured and tailored for each module: occurrence, cloud-base, and fraction (or fraction-thickness) estimation. Each module's structure is defined by the number of neurons in its hidden layers were integrated, each imbued. For the occurrence module, the structure consists of four hidden layers with 108, 64, 36, and 24 neurons, respectively. The CBH prediction module is similarly structured with four hidden layers, but consisting of 96, 56, 32, and 24 neurons, respectively. The module for predicting cloud fraction and thickness has a slightly simpler structure, with three hidden layers containing 56, 32, and 24 neurons, respectively.

As the specific configuration, we utilized the ReLU (Rectified Linear Unit) activation function to introduce non-linearity into the DNN. L2 regularization with a strength of 0.01 is applied to mitigate overfitting by penalizing ~~complexity.~~

~~large~~ weights and encouraging simpler models. Batch normalization ~~was~~is implemented at each layer to normalize the inputs, ensuring consistent data distribution ~~throughout the network, thereby~~and stabilizing the learning process. A dropout rate of 0.2 ~~further prevented overfitting by~~ is used to randomly ~~omitting~~omit neuron connections during training, preventing overfitting and encouraging the network to learn more robust features. ~~Training~~The training process was refined with early stopping, ceasing further epochs when the validation loss ceased to improve, and learning rate reduction, systematically decreasing the learning rate upon encountering plateaus in performance improvement. These callbacks were instrumental in honing the model's performance, ensuring convergence to the accurate ~~representation~~estimation of the BLC. Neuron biases are included in the network's architecture and systematically inserted in the hidden layers (Battaglia et al. 2018). The model is compiled using the Adam optimizer with an initial learning rate of 0.01. The loss functions used are mean squared error for regression tasks and Binary Cross-Entropy for binary classification tasks. The batch size during training is set to 32. Early stopping with a patience of 37 epochs is implemented to prevent overfitting and to restore the best weights when the validation loss ceases to improve.

3.~~2~~3 Model Training Process and Examples

The construction of ~~our~~the deep learning model ~~suite commenced~~commences with the segregation of the ~~comprehensive dataset, sourced from the rich datasets of~~ ARM ~~program,~~observations into a training subset (70%) and a validation subset (30%) during 1998-2016. ~~Additionally~~In addition, we ~~incorporate datasets~~save data from 2017-2020 ~~as part of our validation process~~for testing, specifically focusing on ~~data from the untrained~~this independent period to assess the model's performance. ~~The training and validations are both using the more than 20-year BLC observations, as well as the ARMBE products. The base of BLC is determined at the lowest altitude where cloud fraction exceeds 1%, and the cloud top is identified at the point where cloud fraction transitions from exceeding 1% to falling below this threshold. In multi-layer systems, the DNN model is trained based on the lowest cloud layer when it is coupled with the land surface.~~ Upon training completion, the model ~~was~~is then evaluated, with its performance metrics examined for accuracy and reliability. This methodical and data-driven process ~~balanced~~balances complexity with precision, culminating in a robust model capable of simulating BLC features.

~~These models~~The modules within the deep learning model operate synergistically, with the predicted ~~cloud trigger~~occurrence of clouds extending into the ~~models~~modules for cloud ~~position~~base and the vertical structure (i.e., ~~cloud fraction and~~cloud thickness and shape of the cloud fraction profile). As the example of the model output, Figure 2 offers a comparative display of diurnal cloud fraction profiles over the SGP, contrasting the observed data with the simulated clouds by the deep learning ~~simulations~~model.

443 The model accurately simulates the cloud occurrence and ~~cloud base~~the CBH for these

444 cases, aligning well with observations. However, it falls short in simulating the cloud

445 top ~~position~~heights, especially significant overestimates for stratiform clouds~~,~~

446 ~~overestimating cloud tops.~~. It also underestimates maximum cloud fractions for the

447 stratiform clouds. The observed maximum cloud fraction for stratiform is close to 1,

448 indicating complete coverage, however, such an aspect is not fully replicated by the

449 deep learning model. The third case also falls into the category of stratiform clouds,

450 characterized by ~~a~~an observed cloud fraction exceeding 0.9. However, the presence of

451 multiple local maxima within the cloud fraction profile indicates a relatively complex

452 structure. This complexity poses a challenge to the model, as the DNN is not fully

453 capable of capturing the internal variations within the convective system. Instead, the

454 model tends to produce a more uniform cloud fraction across this convective system.

455 Despite these variances, the model-derived cloud bases and occurrence

456 ~~demonstrates~~demonstrate high consistency with observations, highlighting its value in

457 the cloud simulations.

458

459 **3.~~3~~4 Calculations of Feature Importance and Performance Metric**

460 To elucidate the significance of each input variable within our deep learning models,

461 we implemented a permutation importance analysis. This robust, model-agnostic

462 technique assesses each feature's influence on the model's predictive accuracy, which

463 is crucial for assessing DNN (Date and Kikuchi, 2018; Altmann et al. 2010). In this

464 study, the permutation importance method differs slightly for each module within the

465 deep learning model based on whether the ~~model's~~module's task is regression (cloud

466 ~~position~~base and fraction-thickness) or classification (~~trigger~~occurrence).

467 For the ~~models predicting~~modules of cloud ~~position~~base and ~~cloud~~fraction-

468 thickness, which are regression tasks, the Mean Absolute Error (MAE) serves as the

469 performance metric. First, we perform a test run to establish a baseline performance by

470 calculating the MAE of the ~~model~~module using the original, unperturbed validation

471 datasets, which ~~comprises~~comprise early-morning sounding ~~and~~, surface ~~meteorology~~

472 ~~data~~conditions and the derived variables as the ~~input~~inputs. Then, for every input

473 feature in the validation set, we disrupt its association with the target cloud fields by

474 shuffling its values across all instances, creating a permutation of the dataset. This is

475 executed while maintaining the original order of ~~all other features. Furthermore, we~~

476 ~~recalculate the MAE with the shuffled data.~~other features. When performing the

477 permutation, we shuffle the entire morning profile for each case without altering the

478 internal height order of values within the profile. This approach ensures that while

479 profiles are permuted across different cases, the sequential structure of height values

480 within each profile remains intact. This method allows us to assess the importance of

481 the profiles as coherent units, rather than disrupting their vertical structures.

482 Furthermore, we re-run the DNN modules with the shuffled feature and all other

483 features intact as inputs and recalculate the MAE with the new outputs. The difference

484 between this new MAE and the baseline MAE represents the feature's importance. To

485 ensure a comprehensive assessment, the permutation and the subsequent MAE

486 calculation are repeated 20 times with different random shuffles for each input feature.

487 The final importance score for each feature is then determined as the mean increase in

488 MAE across these permutations.

489 ~~However, for~~For the ~~model classifying~~module of cloud ~~triggers~~occurrence, which

490 is a classification task, the accuracy score is used as the performance metric. The

491 accuracy score is a measure of the model's overall correctness and is calculated using

492 the formula:

493
$$Accuracy = \frac{TP + TN}{TP + TN + FP + FN} \qquad (1)$$

494 where True Positives (TP) indicates the number of instances correctly predicted as

495 positive; true Negatives (TN) indicates the number of instances correctly predicted as

496 negative; False Positives (FP) indicates the number of instances incorrectly predicted

497 as positive, and False Negatives (FN) indicates the number of instances incorrectly

498 predicted as negative. After determining the performance metric, other procedures for

499 determining feature importance remain the same between regression tasks and the

500 classification task. ~~In the model, we filter individual input parameters from the~~

501 ~~consideration of importance score.~~

502 After determining the importance scores from the test run, in refining the model,

503 features contributing a negligible or negative effect on performance (i.e., importance

504 scores less than zero) are excluded to ensure only beneficial data is used.

505 By using this methodology, Figure 3 illustrates these importance scores from

506 different features, underscoring the most influential factors for predicting the ~~presence,~~

507 ~~position~~BLC occurrence, the cloud-base, and the thickness and the shape of the vertical

508 fraction of BLCs. These factors are ranked from most important factors to least

important factors. ~~BLC trigger is a special factor since it is the output of the classification model.~~ Notably, the importance scores are not computed as a simple sum but are determined by collectively shuffling groups of features and observing the impact on model performance. ~~Table 1 complements Figure 3 by providing the model's structure and the precise importance values assigned to each feature across the three cloud prediction tasks. Among these factors, LCL is derived from the surface meteorology (Romps, 2017), BLH_{parcel} is derived from the morning temperature profiles and surface air temperature based on the Parcel method (Holzworth, 1964; Su et al.~~ The BLC trigger of occurrence is a special factor since it is the output of the classification model. The trigger value, which indicates the likelihood of cloud occurrence, is used as an input to the estimations of cloud boundaries and fractions. Sometimes, the trigger value hovers around 0.5, indicating uncertainty about the presence of clouds. This situation often corresponds to scenarios like broken clouds or residual clouds, typically associated with relatively small cloud fractions. Incorporating the trigger value as an input for cloud fraction estimation helps the model account for these ambiguous situations, thereby enhancing its ability to estimate cloud fraction. Specifically, only trigger values greater than 0.5 indicate cloud presence and are used for cloud fraction predictions. While including the trigger value is beneficial for the cloud fraction model, it does not affect the CBH estimation. ~~2020). Specifically, BLH_{parcel} is defined as the height where the morning potential temperature profile first exceeds the current surface potential temperature by more than 1.5 K. BLH_{SH} is derived from the morning temperature profiles and surface sensible heat (Stull, 1988; Su et al. 2023).~~

In particular, surface relative humidity (RH), surface air temperature (T), and morning relative humidity profiles are highly influential in BLC simulations. This is consistent with previous observational and modeling studies (Zhang and Klein, 2013). Surface RH is a critical factor affecting the ~~trigger~~occurrence, CBH, and cloud fraction predictions. As the ~~boundary condition~~input conditions for the DNN ~~model,~~ modules, early-morning atmospheric profiles of different meteorological parameters (i.e., RH, temperature, and wind components) exert a notable impact on cloud ~~trigger~~occurrence detection and the determination of cloud fractions. Surface air temperature is shown to have a substantial effect on cloud fraction, highlighting the sensitivity of cloud simulations to near-surface thermal conditions. ~~This approach~~Meanwhile, BLH_{parcel} demonstrates a notable impact, which is understandable since the PBLH is a critical factor for the formation of BLCs, and BLH_{parcel} provides a good representation of PBLH. This approach also recognizes the interconnectedness of certain features and their collective contribution to the model's output.

4 ~~Modeling~~Boundary Layer Cloud Simulations by the Deep Learning Model

4 4.1 The Occurrence of Boundary Layer Clouds ~~with Deep Learning~~

~~4.1 Boundary Layer Clouds Trigger~~

The occurrence of BLC is a multifaceted process influenced by a variety of atmospheric parameters and surface processes. ~~The BLC trigger,~~As a critical component in the formation of BLCs, ~~is a dynamic phenomenon that our~~ we utilize the deep learning model ~~seeks~~ to identify ~~and simulate from the surface meteorology.~~

553   ~~By~~the BLC trigger using ~~the~~ morning ~~SONDE~~meteorological profiles and

554   ~~measurements of~~observed surface meteorology and fluxes~~,~~. Figure 4 showcases the

555   model's proficiency in classifying the occurrences (class 1) and non-occurrences (class

556   0) of BLC during both a trained period and an ~~untrained, future~~independent period. The

557   classification significantly affects the statistical estimation of cloud fraction, as cloud

558   fraction is set to 0 if the trigger is less than 0.5. The confusion matrices (Luque et al.

559   2019) for the trained period (1998-2016) and for the ~~untrained~~independent period

560   (2017-2020) display the model's predictive performance. The matrices reveal the counts

561   and percentages of TP, FP, TN, and FN. For the training period, we use a 70% training

562   and 30% validation split to ensure model validation and use the validation dataset to

563   generate the statistics. Meanwhile, for the independence period, we use the full dataset

564   for the validation.

565   Figure 4a represents the trained period, ~~we use 30% dataset for~~ the validation ~~and~~

566   ~~see~~datasets show a high percentage of TN at 71.2% and TP at 21.1%, indicating that the

567   model is accurate during the period it was trained ~~on~~. For the ~~untrained~~independent

568   period (2017-2020), the model still performs well, with 71.8% TN and 17.4% TP

569   (Figure 4b). However, the rates of FN and FP are slightly higher at 5.6% and 5.2%

570   respectively, which could indicate that the model is slightly less accurate when applied

571   to data beyond its training scope.

572   ~~TP, FP, TN, and FN, further offer insights into the model's precision, recall, and~~

573   ~~overall accuracy in detecting the presence of BLC. Precision, which gauges the~~

574 ~~accuracy of positive predictions, recall, which assesses the detection of actual positives,~~

575 ~~and the F1 score, which balances the two, are consistently above 75% across both~~

576 ~~periods. This high performance across key metrics demonstrates the model's robustness~~

577 ~~and reliability in identifying the onset of BLCs.~~

578 ~~Table 2 complements the Figure 4 and provides a detailed quantitative number of~~

579 ~~the model's classification performance. It presents the number of instances and their~~

580 ~~corresponding percentages of different matrices (i.e., TN, FP, FN, and TP). The high~~

581 ~~percentages of correct predictions (TP and TN) underscore the model's effectiveness,~~

582 ~~while the lower FP and FN rates reflect its reliability.~~ The table highlights the model's

583 robustness, with overall accuracy rates of 92.3% for the trained period and a slightly

584 reduced but still substantial 89.2% for the ~~untrained period.~~ independent period.

585 Moreover, for the trained period, the model achieved a high precision of 88.1% and a

586 recall of 81.2%. For the independent period, the precision and recall remained

587 reasonably high at 76.9% and 75.6%, respectively, demonstrating the model's effective

588 generalization to new data. These metrics demonstrate the model's predictive

589 capabilities and reliability for both trained and ~~untrained~~ independent periods.

590 Figure 5 further compares the diurnal frequency of BLC occurrence between

591 observations (OBS) and the DNN predictions for different seasons. The BLC's strong

592 diurnal pattern is well-captured by the model, when BLC development peaks between

593 12-16 local times, aligning closely with observed frequencies. Among different seasons,

594 the model is notably effective in simulating the pronounced diurnal cycle of summer

595 clouds, which are typically influenced by local convection. Conversely, the winter

season exhibits a weaker diurnal pattern, likely ~~linking~~linked to the diminished surface

fluxes. The DNN tends to overestimate BLC presence in the early morning, especially

for the winter season. The overall alignment between observations and the DNN

~~model~~module represents the model's capability of capturing the diurnal patterns of BLC

formation and development. Determining the ~~triggers~~occurrence of BLC lays the

foundation for the integrated simulations of BLC features.

4.2 ~~Simulating~~ Cloud ~~Positions~~Boundaries and ~~Cloud Fractions~~Fraction

A key aspect of cloud modeling involves the accurate simulation of cloud

~~positions~~boundaries and ~~fractions~~fraction, which are indicative of a cloud's vertical

extent and fractional coverage at different height levels. Our deep learning model

demonstrates capabilities in predicting these key attributes of BLC.

Figure 6 offer the comparisons between observed values and predictions by the

DNN for CBH, CTH, and cloud fraction. ~~These~~Similarly, as in Section 4.1, these

comparisons are presented for both the training period (a, c, e, based on validation

datasets) and an independent period (b, d, f), revealing the model's ability to generalize

beyond its initial training data. The DNN model demonstrates remarkable performance

in simulating cloud base, boasting a correlation coefficient surpassing 0.9 and an MAE

under 0.15 km. Conversely, the model encounters challenges with CTH prediction,

evidenced by a lower correlation of about 0.5 and a significantly higher MAE between

0.8 and 0.9 km, aligning with case studies in Figure 2.

617   The discrepancy in accurately simulating CBH and CTH may stem from two main

618   factors. Firstly, observed CBH determinations are generally more precise due to the

619   effectiveness of laser-based methods (Pal et al., 1992), while observed CTH estimations

620   often suffer from reduced accuracy, partly attributed to signal attenuation issues

621   (Clothiaux et al., 2000). For the observed shallow cumulus, cloud top is often

622   contaminated by insect signals, further complicating accurate CTH measurements

623   (Chandra et al, 2010). Secondly, our DNN simulations are developed from the

624   perspective of cloud-land coupling, primarily utilizing surface meteorology. This can

625   introduce inherent limitations, as the tops of many clouds may be decoupled from

626   surface influences despite a coupled base, potentially leading to potential gaps in the

627   model's parameterizationDNN's ability to accurately define and estimate the cloud top.

628   The comparison of cloud fraction between observations and DNN areis presented

629   to consider the model's capability to simulate the vertical distribution of cloud coverage

630   (Figure 6e-f). The scatterplots comparing observed and modeled cloud fractions at

631   individual levels in cloudy scenarios show a satisfactory correlation, with an R-value

632   exceeding 0.77 and an MAE around 0.15. Nevertheless, the DNN model tends to

633   underestimate the peak cloud fraction, displaying a range up to ~0.8 compared to the

634   full 0-1 range observed. This underestimation is intrinsically linked to the model's

635   simulation of cloud positionboundaries, as both cloud fraction and position

636   modelscloud-base modules operate in tandem. For stratiform clouds, observational data

637   typically exhibit a relatively uniform vertical extent with cloud fractions close to unity

638   at the central height, whereas the DNN model tends to generate a broader, more

639   attenuated profile with a reduced maximum cloud fraction at the center. This points to

640   a need for refining the model's ability to replicate the pronounced peak cloud fractions

641   characteristic of stratiform cloud profiles.

642   The diurnal patterns of cloud base and top heights, captured through daily profiles,

643   showcase the model's adeptness at simulating the temporal changes in cloud positions

644   for all BLCs, the cumulus regime, and the stratiform regime (as shown in Figure 7).

645   These profiles, derived from both observational data and DNN outputs, include shaded

646   regions representing the variability (one standard deviation) around the average heights.

647   Cumulus clouds exhibit a marked diurnal cycle, whereas stratiform clouds typically

648   maintain a relatively ~~consistent position~~constant cloud boundaries and smaller

649   variations throughout the day. A close alignment is observed between the mean and

650   standard deviation of the cloud base between the observed and the simulated data for

651   different cloud regimes. In contrast, while the mean cloud top heights follow a similar

652   diurnal trend in both cases, the ~~variability presented by the~~ observed data exhibits more

653   pronounced variabilities compared to the relatively small variabilities in the DNN

654   simulations.

655   Figures 6 and 7 collectively demonstrate the model's ability to simulate cloud

656   ~~positions~~boundaries and fractions within BLC. It reliably captures ~~cloud base~~

657   ~~heights~~CBH yet encounters challenges with accurately representing cloud top heights

658   and peak cloud fractions on an individual basis. These constraints are somewhat

659   expected, given that even very fine-scale ~~model~~models struggle to entirely capture the

660 vertical extent of clouds, as evidenced in Large-Eddy Simulations or Convection-

661 Permitting Models (Zhang et al. 2017; Gustafson et al. 2020; Bogenschutz et al. 2023).

662 In addition to the discussion of deep learning models, we also acknowledge the role of

663 mixed-layer (single-column) models in representing boundary layer processes (Lilly

664 1968, Pelly and Belcher, 2001; Clayson and Chen, 2002; Zhang et al, 2005, 2009; De

665 Roode et al., 2014). Mixed-layer models have several advantages: they are inherently

666 grounded in physical principles and are readily integrated into many large-scale models.

667 These models are effective at capturing the diurnal evolution of the PBL given an initial

668 state and time series of surface fluxes. However, the DNN approach offers distinct

669 benefits that complement this theoretical approach. DNNs might be able to capture

670 complex, nonlinear relationships between various controlling factors and the cloud

671 fraction. These~~is~~ may be difficult to capture by the single (for the overcast

672 stratocumulus-topped mixed layer) or multiple mixed-layer models (for the broken

673 trade cumulus clouds), which are still subject to assumptions, e.g., on entrainment

674 processes. By training on large observational datasets, DNNs can learn from real-world

675 examples, potentially identifying patterns and relationships not explicitly encoded in

676 physical models.

677

678 5 ~~Integrating~~ Application of the Deep Learning ~~Models into~~
679  Model

680 ~~4.3~~5.1 Integration with Reanalysis Datasets

681 ~~The DNN~~As shown in Section 4, the deep learning model can ~~use~~take the

conventional meteorological ~~data~~observations (i.e. morning SONDE and surface ~~meteorology data)~~conditions) as inputs to ~~diagnose~~simulate the BLC~~. Meanwhile, as~~ outputs, reasonably reproduce a good agreement with the observed vertical structures of BLCs. For its potential application, we may treat it ~~also can be used in reanalysis data (i.e.,~~as an "emulator" of the observed relationships between input and output variables. Here we present an example by integrating the deep learning model with ERA-5 and MERRA-2~~) to serve as the convection parameterization~~ to simulate BLC with the input of early-morning profiles and ~~meteorology data~~surface conditions from the reanalysis. ~~Thus, we can assess the integration of Deep Learning Models with reanalysis datasets to refine the simulation of BLCs.~~Here we ask, if inputs are treated as "reality", what would be the expected responding cloud fraction simulated by the deep learning model, an observation-based emulator?

Following ~~this~~these thoughts, Figure 8 contrasts diurnal cloud fraction patterns from the observational data and the deep learning model predictions ~~across~~averaged over all conditions of seasons and years. Figure 8a-b present the observed cloud fractions and those simulated by ~~our~~the deep learning ~~neural network (DNN),~~using ARM data as inputs, respectively. Panels c and e ~~display~~show the cloud fractions directly ~~available~~extracted from ERA-5 and MERRA-2 reanalysis datasets, while panels d and f illustrate the ~~enhanced simulation results after the application of DNN to~~simulated cloud fraction by the deep learning model using inputs from ERA (ERA_{DNN}) and MERRA ($MERRA_{DNN}$) ~~data. To eliminate sampling biases, we averaged only those samples for which both observational and~~ reanalysis ~~datasets are concurrently~~

704 ~~available~~data. Observing fluctuations in surface temperature and humidity data in ERA-

705 5 for this region, we smoothed ERA-5 surface air temperature and humidity data with

706 a $\pm$1-hour window to mitigate potential variability from assimilation before using them

707 as input for the DNN~~.~~ modules. To eliminate sampling biases in comparison, we

708 averaged only those samples for which both observations and reanalysis are

709 concurrently available.

710 Note that here we adopt the deep learning model as a complementary tool rather

711 than a replacement for any existing cloud representations in reanalysis data. The DNN

712 outputs serve a diagnostic purpose, identifying biases in BLCs and aiding in

713 understanding deficiencies within reanalysis data.

714 The DNN simulations with ~~observed meteorological data~~ARM observations as

715 inputs align closely ~~in~~with the ARM observed cloud fraction profiles within the 0-2 km

716 range, reflecting the model's ability to capture land-coupled clouds. As this model ~~are~~is

717 designed for diagnosing land-coupled clouds, the model does not simulate decoupled

718 clouds, which often have bases occurring above ~~the~~ 2-km (Su et al. 2022). Original

719 cloud data directly from reanalysis ~~data~~ show significant underestimations of ~~cloud~~BLC

720 fractions ~~for low clouds~~, particularly evident in MERRA-2. The

721 ~~implementation~~application of ~~DNN~~the deep learning model using reanalysis data as

722 inputs enhances cloud fraction ~~representation~~estimations compared to the original cloud

723 data directly from reanalysis ~~data~~, demonstrating the DNN model's strength in

724 simulating BLC. Given that the DNN model specializes in simulating BLC, when

725 utilizing reanalysis data, the portion of cloud profiles that are decoupled are preserved

as they are in the original datasets—that is, for the cloud layers above the BLC-tops or ~~for~~as those clouds ~~that~~ rooted above the PBL.

Furthermore, Figure 9 provides a detailed examination of stratiform clouds, utilizing the same comparative approach as in Figure 8. The observed stratiform clouds display a layered structure with expansive coverage and maximum cloud fractions typically exceeding 0.6. The DNN model ~~reproduce~~using ARM data as inputs reproduces these observed characteristics fairly well, albeit with minor overestimations in cloud vertical extent. Conversely, the original ERA-5 and MERRA-2 stratiform cloud data exhibit limitations, particularly in underestimating cloud fraction. The integration of the DNN model with reanalysis data as inputs enhances the ~~representation~~estimations of stratiform cloud fractions, as depicted in the heatmaps of Figure 9, showcasing improved agreement with observational data and underscoring the enhancement potential for cloud fraction simulations in reanalysis datasets.

~~Additionally~~In addition, Figure 10 extends the comparative study to cumulus clouds. Cumulus clouds pose significant challenges for modeling and parameterization partly due to their typically small spatial extent compared to the model grid, often spanning from a few hundred meters to several kilometers (Zhang et al. 2017; Tao et al., 2021; Bogenschutz et al. 2023; Gustafson et al. 2020). In line with expectations, the original ERA-5 and MERRA-2 cloud fields exhibit significant biases in representing cumulus clouds when compared to observational data~~, possibly related to the large grid of the reanalysis that might not fully capture the fine-scale characteristics of cumulus formations.~~

. In contrast, the DNN model with ARM data as inputs achieves commendable success in capturing the diurnal variability of cumulus clouds, including cloud base, vertical extension, and cloud fraction, by leveraging local convective signals derived from surface meteorology data. When the DNN methodologymodel is applied tointegrated with ERA-5 as inputs, it significantly improves the representationestimation of vertical cloud fields of cumulus clouds. However, the original MERRA-2 data, which tend to overlook the majority of cumulus clouds, continue to significantly underrepresent them even after the application of DNN, suggesting that additional biases in the input variables such as meteorological factors may contribute to this discrepancy.

The integration of deep learning with ERA-5 and MERRA-2 reanalysis datasets demonstrates the notable refinement in the simulation of BLC. By integrating our deep learning models with reanalysis data, we achieve a, and achieves more accurate representationestimations of cloud fractions for both stratiform and cumulus clouds.

4.45.2 Applying Deep Learning for Bias Attribution in Cloud Simulation

We further examine the remaining disparities in cloud fraction simulations within reanalysis datasets, despite the integration of deep learning models (as shown in Figures 8-10), indicating persisting meteorological biases. Deep learning is utilized to quantify and attribute these biases for BLC simulations.

Figure 11 offers a comparative analysis of vertical cloud fraction profiles for both stratiform and cumulus clouds. It presents cloud fractions observed with thosedirectly

taken from reanalysis data (RD), including ERA-5, and MERRA-2, and their corresponding deep learning-informed simulations. While the application of deep learning to use reanalysis data as inputs (RD$_{DNN}$) yields improvements, remaining cloud biases are evident, particularly in MERRA-2. Acknowledging the significant influence of surface RH on BLC simulations (as indicated by Figure 3e, inputwe refine the inputs into the DNN model by replacing the reanalysis surface RH with the ARM observed surface relative humidity (RH) instead of reanalysis RH into (the DNN models (themodel output is labeled as RD$_{DNN-RH}$). This modification leads to a more accuratemuch better simulation for MERRA-2, closing the gap with observational data, especially for stratiform clouds. For ERA-5, RD$_{DNN-RH}$ and RD$_{DNN}$ show negligible differences for cumulus clouds, but for stratiform clouds, RD$_{DNN-RH}$ also exhibits a reduced bias. These refined profiles of cloud fraction attest to the benefits of using the observed surface moisture data as input, confirming its important role in achieving a more accurate representation of BLC.

We canWith such methodology, we may further dissect the bias in cloud fraction simulations attributed to various meteorological factors and the parameterization schemes within ERA and MERRA reanalysis datasets:

$$Bias\ due\ to\ parameterization = |RD - OBS| - |RD_{DNN} - OBS| \qquad (2)$$

$$Bias\ due\ to\ surface\ RH = |RD_{DNN} - OBS| - |RD_{DNN-RH} - OBS| \qquad (3)$$

where RD and OBS are the cloud fraction derivedtaken directly from reanalysis data and observations, respectively. The definitiondefinitions of RD$_{DNN}$ and RD$_{DNN-RH}$ are the same withas the above. For getting a representative value, these biases are layer-

averaged from 0-4 km over different local times, and then normalized by the observed

mean cloud fraction, offering a climatological perspective on the discrepancies between

observed and simulated data across seasons and years. For equation (2), we assume that

the climatology of observations used as input to the DNN model (OBS$_{DNN}$) matches the

observed cloud fraction climatology (i.e., OBS$_{DNN}$≈OBS), which has been

demonstrated in Figures 9-11. Therefore, we exclude the term representing the

difference between the DNN-predicted observations and the actual observations. This

assumption justifies our approach by ensuring the input observations align with the

observed cloud fraction in equations.

We get the bias attributed to different meteorological factors and parameterization

schemes in the ERA-5 and MERRA-2 datasets, respectively (Figure 12). Each ~~bars~~

~~indicate~~bar indicates the normalized bias contributed by factors such as morning

meteorological profiles, surface pressure, surface fluxes, various surface meteorology

variables, and parameterization schemes. Notably, parameterization stands out as a

significant contributor to bias, accounting for 14.45~~%/~~% and 19.05% of the discrepancy

in stratiform clouds between observations ~~and~~versus ERA-5~~/~~ and MERRA-2

respectively. For cumulus clouds, the parameterization biases are more pronounced,

contributing 22.23% and 30.94% for ERA-5 and MERRA-2, respectively.

In addition to parameterization, RH, RH profiles, and sensible heat are identified as

major factors contributing to the differences between observations and reanalysis data.

For instance, aligning MERRA-2's RH with observed surface RH could potentially

reduce bias by 23.13% for stratiform and 10.26% for cumulus clouds. Meanwhile,

814 surface RH and morning RH profiles in ERA-5 lead to 11.25% and 3.96% of biases for

815 the stratiform clouds. The bias between ERA-5 and observed cumulus clouds is largely

816 driven by parameterization, which suggests that employing the DNN model with ERA-

817 5 can lead to a more accurate simulation of cumulus clouds.

818   The detailed bias attribution analysis facilitated by the deep learning model

819 elucidates the individual impact of meteorological factors on the discrepancies in cloud

820 fraction between observations and reanalysis data. It underscores the necessity for more

821 accurate humidity data within reanalysis datasets to refine BLC simulations.

822 Furthermore, this deep learning approach illuminates pathways for improved

823 parameterization of boundary layer convection.

824

825 **56. Summary**

826   This study has developed a deep learning model to estimate the evolution of BLCs

827 over the SGP. The model utilizes over two decades of meteorological data to simulate

828 BLC formation and characteristics, including ~~timing~~the occurrence of ~~convection~~

829 ~~initiation (BLC onset), their positions~~BLCs, cloud boundaries, and vertical structures

830 of cloud fraction. As this model is built based on the perspective of cloud-land coupling,

831 the DNN approach demonstrates the capability to diagnose land-coupled convective

832 systems from early-morning sounding and surface ~~meteorology~~conditions. The DNN

833 model is built on the cloud-land interactions and serves as the testimony for the coupling

834 between BLCs and the land surface. The proficiency and reliability of the DNN model

835 ~~is~~are evident in its robustness during both the training period and the subsequent

independent periods. The deep learning model addresses the simulation of cloud vertical structure, among one of the key challenges in physics-based large-scale models. It should be noted that the current DNN model cannot produce detailed cloud microphysics and turbulence information. We propose using the DNN model alongside traditional physical models to obtain comprehensive information on BLCs.

The implementationapplication of this model withinon the reanalysis datasets like ERA-5 and MERRA-2 has resulted in enhanced representationcloud field estimations for stratiform clouds and cumulus, and an accurate vertical structure of clouds in termterms of climatology, providing a promising diagnostic tool for improving weather forecasting and climate modeling. The deep learning model notably addressaddresses the limitation in cumulus simulations in the reanalysis data, Meanwhile, this approach is much more cost-effective compared to traditional parameterizations and schemes at various scales, as it can simulate two decades of BLCBLCs with vertical information over the SGP in ~30 secondwithin 1-minute using a single GPU node.

In addition to the BLC simulations, the deep learning model developed in this study also is used to attribute discrepancies between observational data and reanalysis datasets to different meteorological factors. Besides parameterization, surface RH, morning RH profiles, and surface sensible heat are the three major factors that lead to the mismatches in BLC representation in ERA-5 and MERRA-2. These findings underscore the importance of incorporating more accurate humidity information in reanalysis datasets, which is crucial for refining BLC simulations. This analysis also sheds light on the necessity to update reanalysis datasets with improved

parameterization of boundary layer convection.

~~By leveraging deep learning, the model addressed the simulation of cloud vertical structure, among one of the key challenges in the field. They highlight the value of deep learning in advancing our understanding of BLC dynamics and improving the representation of low clouds in atmospheric models. This work not only narrows the observational-modeling divide but also paves the way for future developments in cloud parameterization. Moving forward, future work is warranted to test and extend this parameterization to different synoptic regions. The goal is to develop a versatile model capable of simulating BLC on a global scale, which can be integrated into multiple scale models or reanalysis data.~~ Moving forward, future work is warranted to test and extend this diagnostic tool to different synoptic patterns over a large region, which can be integrated into multiple-scale models or reanalysis data. However, several challenges need to be addressed to achieve this. One significant limitation is the lack of high-quality, detailed observations of clouds and radiosonde profiles globally. This scarcity of data can hinder the model's ability to generalize effectively across different regions. To overcome this, there are several potential strategies. First, using transfer learning techniques can help adapt the model trained in one region to other regions with limited data. Integrating data from global observational networks (i.e., ARM) can also create a more diverse and representative training dataset, capturing a wider range of atmospheric conditions and cloud characteristics. Meanwhile, leveraging satellite data can provide broader coverage and enhance the robustness of the model. We plan to explore these approaches in future work to enhance the model's performance and applicability on a

880 global scale.

881

882

883 ***Code and data availability.*** The code package of DNN models and for the ~~The~~

884 simulation outputs of BLCs from observed meteorological data and ERA-5 and

885 MERRA-2 is available under the GNU General Public License v3.0 at ~~can be found in~~

886 https://doi.org/10.5281/zenodo.10719342 (Su, 2024). ARM radiosonde data, surface

887 fluxes, and cloud masks are available at

888 https://adc.arm.gov/discovery/#/results/instrument_class_code::armbe (ARM user

889 facility, 1994). ARSCL (Active Remote ~~Sesning~~Sensing of ~~Cloud~~Clouds) can be found

890 in https://adc.arm.gov/discovery/#/results/instrument_class_code::arscl (ARM user

891 facility, 1996). MERRA-2 reanalysis data can be downloaded obtained from

892 https://disc.gsfc.nasa.gov/datasets/M2T1NXRAD_5.12.4/summary?keywords%E2%8

893 0%89=%E2%80%89MERRA-2%20tavg1_2d_rad_Nx (GMAO, 2015). ERA-5

894 reanalysis data are obtained from

895 https://cds.climate.copernicus.eu/cdsapp#!/dataset/reanalysis-era5-pressure-

896 levels?tab=form (Hersbach et al. 2023).

897

898 ***Author contributions.*** TS designed this study and carried out the analysis and model

899 training. TS and YZ interpreted the data and wrote the manuscript. YZ supervised the

900 project.

901

902 ***Competing interests.*** The contact author has declared that neither they nor their co-

903 authors have any competing interests.

904

Acknowledgements. Work at LLNL is performed under the auspices of the U.S. DOE

by Lawrence Livermore National Laboratory under Contract DE-AC52-07NA27344.

This research used resources of the National Energy Research Scientific Computing

Center (NERSC), a U.S. Department of Energy Office of Science User Facility located

at Lawrence Berkeley National Laboratory, operated under Contract No. DE-AC02-

05CH11231. We acknowledge the the U.S. Department of Energy's ARM program for

offering the comprehensive filed observations.

Financial support. This work has been supported bythe DOE Atmospheric System

Research (ASR) Science Focus Area (SFA) THREAD project (SCW1800).

References

Altmann, A., Toloşi, L., Sander, O. and Lengauer, T.: Permutation importance: a corrected feature importance measure. Bioinformatics, 26(10), pp.1340-1347., 2010.

Atmospheric Radiation Measurement (ARM) user facility.: ARM Best Estimate Data Products (ARMBEATM). Southern Great Plains (SGP) Central Facility, Lamont, OK (C1). Compiled by C. Xiao and X. Shaocheng. [Dataset] ARM Data Center. Dataset accessed 2023-12-25 at http://dx.doi.org/10.5439/1333748., 1994.

Atmospheric Radiation Measurement (ARM) user facility.: Active Remote Sensing of CLouds (ARSCL1CLOTH). 2024-02-05 to 2024-02-13, Southern Great Plains (SGP) Central Facility, Lamont, OK (C1). Compiled by S. Giangrande, D. Wang, E. Clothiaux and P. Kollias. [Dataset] ARM Data Center. Dataset accessed 2023-12-25 at http://dx.doi.org/10.5439/1996113., 1996.

Battaglia, P.W., Hamrick, J.B., Bapst, V., Sanchez-Gonzalez, A., Zambaldi, V., Malinowski, M., Tacchetti, A., Raposo, D., Santoro, A., Faulkner, R. and Gulcehre, C.: Relational inductive biases, deep learning, and graph networks. arXiv preprint arXiv:1806.01261., 2018.

Berg, L. K., and Kassianov, E.I.: Temporal variability of fair-weather cumulus statistics at the ACRF SGP site. J. Climate, 21(13), 3344–3358., 2008.

Betts, A.K.: Land‐surface‐atmosphere coupling in observations and models. Journal of Advances in Modeling Earth Systems, 1(3)., 2009.

Bogenschutz, P. A., Eldred, C., & Caldwell, P. M.: Horizontal resolution sensitivity of the Simple Convection-Permitting E3SM Atmosphere Model in a doubly-periodic configuration. Journal of Advances in Modeling Earth Systems, 15, e2022MS003466. https://doi.org/10.1029/2022MS003466, 2023.

Bretherton, C. S., Blossey, P. N., and Uchida, J.: Cloud droplet sedimentation, entrainment efficiency, and subtropical stratocumulus albedo. Geophys. Res. Lett., 34(3), L03813., 2007.

Cadeddu, M. P., Turner, D. D., and Liljegren, J. C.: A neural network for real-time retrievals of PWV and LWP from Arctic millimeter-wave ground-based observations, IEEE T. Geosci. Remote, 47, 1887–1900., 2009.

Caldwell, P.M., Terai, C.R., Hillman, B., Keen, N.D., Bogenschutz, P., Lin, W., Beydoun, H., Taylor, M., Bertagna, L., Bradley, A.M. and Clevenger, T.C.: Convection‐permitting simulations with the E3SM global atmosphere model. Journal of Advances in Modeling Earth Systems, 13(11), p.e2021MS002544., 2021.

Chandra, A. S., Kollias, P., Giangrande, S. E., & Klein, S. A.: Long-term observations of the convective boundary layer using insect radar returns at the SGP ARM climate research facility. Journal of climate, 23(21), 5699-5714., 2010.

Clayson, C.A. and Chen, A.: Sensitivity of a coupled single-column model in the tropics to treatment of the interfacial parameterizations. Journal of climate, 15(14), pp.1805-1831., 2002.

Clothiaux, E. E., Ackerman, T. P., Mace, G. G., Moran, K. P., Marchand, R. T., Miller, M. A., and Martner, B. E.: Objective determination of cloud heights and radar reflectivities using a combination of active remote sensors at the ARM CART sites. J. Appl. Meteorol., 39(5), 645–665., 2000.

Clothiaux, E.E., Miller, M.A., Perez, R.C., Turner, D.D., Moran, K.P., Martner, B.E., Ackerman, T.P., Mace, G.G., Marchand, R.T., Widener, K.B. and Rodriguez, D.J.: The ARM millimeter wave cloud radars (MMCRs) and the active remote sensing of clouds (ARSCL) value added product (VAP) (No. DOE/SC-ARM/VAP-002.1). DOE Office of Science Atmospheric Radiation Measurement (ARM) Program (United States)., 2001.

Cook, D. R.: Energy Balance Bowen Ratio (EBBR) instrument handbook, Technical Report Rep. DOE/SC-ARM/TR-037, U.S. Department of Energy., 2018.

Date, Y. and Kikuchi, J.: Application of a deep neural network to metabolomics studies and its performance in determining important variables. Analytical chemistry, 90(3), pp.1805-1810., 2018.

De Roode, S.R., Siebesma, A.P., Dal Gesso, S., Jonker, H.J., Schalkwijk, J. and Sival, J.: A mixed‐layer model study of the stratocumulus response to changes in large‐scale conditions. Journal of Advances in Modeling Earth Systems, 6(4), pp.1256-1270., 2014.

Fast, J. D., Berg, L. K., Alexander, L., Bell, D., D'Ambro, E., Hubbe, J., Kuang, C., Liu, J., Long, C., Matthews, A., and Mei, F.: Overview of the HI-SCALE field campaign: A new perspective on shallow convective clouds, B. Am. Meteorol. Soc., 100, 821–840.: , 2019.

Gagne II, D. J., Haupt, S. E., Nychka, D. W., and Thompson, G.: Interpretable deep

981 learning for spatial analysis of severe hailstorms, Mon. Weather Rev., 147.: 2845,
982   (2019)., 2827.
983 Gelaro, R., McCarty, W., Suárez, M.J., Todling, R., Molod, A., Takacs, L., Randles,
984   C.A., Darmenov, A., Bosilovich, M.G., Reichle, R. and Wargan, K.: The modern-
985   era retrospective analysis for research and applications, version 2 (MERRA-2).
986   Journal of climate, 30(14), pp.5419-5454., 2017.
987 Gentine, P., Pritchard, M., Rasp, S., Reinaudi, G. and Yacalis, G.: Could machine
988   learning break the convection parameterization deadlock?. Geophysical Research
989   Letters, 45(11), pp.5742-5751., 2018.
990 Global Modeling and Assimilation Office (GMAO.: MERRA-2 tavg1_2d_rad_Nx:
991   2d,1-Hourly,Time-Averaged,Single-Level,Assimilation,Radiation Diagnostics
992   V5.12.4, Greenbelt, MD, USA [Dataset]. Goddard Earth Sciences Data and
993   Information Services Center (GES DISC),
994   https://doi.org/10.5067/Q9QMY5PBNV1T., 2015.
995 Golaz, J.C., Larson, V.E. and Cotton, W.R.: A PDF-based model for boundary layer
996   clouds. Part I: Method and model description. Journal of the atmospheric sciences,
997   59(24), pp.3540-3551., 2002.
998 Guo, J., Su, T., Chen, D., Wang, J., Li, Z., Lv, Y., ... & Zhai, P.: Declining summertime
999   local‐scale precipitation frequency over China and the United States, 1981–2012:
1000   The disparate roles of aerosols. Geophysical Research Letters, 46(22), 13281-
1001   13289., 2019.
1002 Guo, J., Zhang, J., Shao, J., Chen, T., Bai, K., Sun, Y., Li, N., Wu, J., Li, R., Li, J. and
1003   Guo, Q.: A merged continental planetary boundary layer height dataset based on
1004   high-resolution radiosonde measurements, ERA5 reanalysis, and GLDAS. Earth
1005   System Science Data, 16(1), pp.1-14., 2024.
1006 Gustafson, W.I., Vogelmann, A.M., Li, Z., Cheng, X., Dumas, K.K., Endo, S., Johnson,
1007   K.L., Krishna, B., Fairless, T. and Xiao, H.: The large-eddy simulation (LES)
1008   atmospheric radiation measurement (ARM) symbiotic simulation and observation
1009   (LASSO) activity for continental shallow convection. Bulletin of the American
1010   Meteorological Society, 101(4), pp.E462-E479., 2020.
1011 Haynes, J.M., Noh, Y.J., Miller, S.D., Haynes, K.D., Ebert-Uphoff, I. and Heidinger, A.:
1012   Low cloud detection in multilayer scenes using satellite imagery with machine
1013   learning methods. Journal of Atmospheric and Oceanic Technology, 39(3), pp.319-
1014   334., 2022.
1015 Hersbach, H., Bell, B., Berrisford, P., Biavati, G., Horányi, A., Muñoz Sabater, J.,
1016   Nicolas, J., Peubey, C., Radu, R., Rozum, I., Schepers, D., Simmons, A., Soci, C.,
1017   Dee, D., Thépaut, J-N.: ERA5 hourly data on pressure levels from 1940 to present.
1018   [Dataset] Copernicus Climate Change Service (C3S) Climate Data Store (CDS),
1019   DOI: 10.24381/cds.bd0915c6., 2023.
1020 Hersbach, H., Bell, B., Berrisford, P., Hirahara, S., Horányi, A., Muñoz‐Sabater, J.,
1021   Nicolas, J., Peubey, C., Radu, R., Schepers, D. and Simmons, A.: The ERA5 global
1022   reanalysis. Quarterly Journal of the Royal Meteorological Society, 146(730),
1023   pp.1999-2049., 2020.
1024 Holdridge, D., Ritsche, M., Prell, J., and Coulter, R.: Balloon-borne sounding system

(SONDE) handbook, https://www.arm.gov/capabilities/instruments/sonde., 2011.

Holzworth, G. C.: Estimates of mean maximum mixing depths in the contiguous United States, Mon. Weather Rev., 92, 235–242, https://doi.org/10.: 1520-0493(1964)092<0235:eommmd>2.3.co;2, 1964., 1175.

Klambauer, G., Unterthiner, T., Mayr, A., & Hochreiter, S.: Self-normalizing neural networks. Advances in neural information processing systems, 30., 2017.

Kollias, P., Bharadwaj, N., Clothiaux, E.E., Lamer, K., Oue, M., Hardin, J., Isom, B., Lindenmaier, I., Matthews, A., Luke, E.P. and Giangrande, S.E.: The ARM radar network: At the leading edge of cloud and precipitation observations. Bulletin of the American Meteorological Society, 101(5), pp.E588-E607., 2020.

Kuma, P., McDonald, A.J., Morgenstern, O., Alexander, S.P., Cassano, J.J., Garrett, S., Halla, J., Hartery, S., Harvey, M.J., Parsons, S. and Plank, G.: Evaluation of Southern Ocean cloud in the HadGEM3 general circulation model and MERRA-2 reanalysis using ship-based observations. Atmospheric Chemistry and Physics, 20(11), pp.6607-6630., 2020.

Lareau, N.P., Zhang, Y. and Klein, S.A.: Observed boundary layer controls on shallow cumulus at the ARM Southern Great Plains site. Journal of the Atmospheric Sciences, 75(7), pp.2235-2255., 2018.

Lee, J.M., Zhang, Y. and Klein, S.A.: The effect of land surface heterogeneity and background wind on shallow cumulus clouds and the transition to deeper convection. Journal of the Atmospheric Sciences, 76(2), pp.401-419., 2019.

Lilly, D.K.: Models of cloud-topped mixed layers under a strong inversion. Q.J.R. Meteorol. Soc., 94: 292-309. https://doi.org/10.1002/qj.49709440106, 1968.

Lu, C., Liu, Y. and Niu, S.: Examination of turbulent entrainment‐mixing mechanisms using a combined approach. Journal of Geophysical Research: Atmospheres, 116(D20)., 2011.

Lu, C., Niu, S., Liu, Y. and Vogelmann, A.M.: Empirical relationship between entrainment rate and microphysics in cumulus clouds. Geophysical Research Letters, 40(10), pp.2333-2338., 2013.

Luque, A., Carrasco, A., Martín, A. and de Las Heras, A.: The impact of class imbalance in classification performance metrics based on the binary confusion matrix. Pattern Recognition, 91, pp.216-231., 2019.

McGovern, A., Elmore, K. L., Gagne, D. J., Haupt, S. E., Karstens, C. D., Lagerquist, R., Smith, T., and Williams, J. K.: Using artificial intelligence to improve real-time decision-making for high-impact weather, B. Am. Meteorol. Soc., 98.: 2090, (2017)., 2073.

Miao, H., Wang, X., Liu, Y. and Wu, G.: An evaluation of cloud vertical structure in three reanalyses against CloudSat/cloud‐aerosol lidar and infrared pathfinder satellite observations. Atmospheric Science Letters, 20(7), p.e906., 2019.

Moeng, C.H., Cotton, W.R., Bretherton, C., Chlond, A., Khairoutdinov, M., Krueger, S., Lewellen, W.S., MacVean, M.K., Pasquier, J.R.M., Rand, H.A. and Siebesma, A.P.: Simulation of a stratocumulus-topped planetary boundary layer: Intercomparison among different numerical codes. Bulletin of the American Meteorological Society, 77(2), pp.261-278., 1996.

Molero, F., Barragán, R. and Artíñano, B.: Estimation of the atmospheric boundary layer height by means of machine learning techniques using ground-level meteorological data. Atmospheric Research, 279, p.106401., 2022.

Mooers, G., Pritchard, M., Beucler, T., Ott, J., Yacalis, G., Baldi, P. and Gentine, P.: Assessing the potential of deep learning for emulating cloud superparameterization in climate models with real‐geography boundary conditions. Journal of Advances in Modeling Earth Systems, 13(5), p.e2020MS002385., 2021.

Morrison, H., van Lier‐Walqui, M., Fridlind, A.M., Grabowski, W.W., Harrington, J.Y., Hoose, C., Korolev, A., Kumjian, M.R., Milbrandt, J.A., Pawlowska, H. and Posselt, D.J.: Confronting the challenge of modeling cloud and precipitation microphysics. Journal of advances in modeling earth systems, 12(8), p.e2019MS001689., 2020.

Nogherotto, R., Tompkins, A.M., Giuliani, G., Coppola, E. and Giorgi, F.: Numerical framework and performance of the new multiple-phase cloud microphysics scheme in RegCM4. 5: precipitation, cloud microphysics, and cloud radiative effects. Geoscientific Model Development, 9(7), pp.2533-2547., 2016.

O'Gorman, P.A. and Dwyer, J.G.: Using machine learning to parameterize moist convection: Potential for modeling of climate, climate change, and extreme events. Journal of Advances in Modeling Earth Systems, 10(10), pp.2548-2563., 2018.

Pal, S.R., Steinbrecht, W. and Carswell, A.I.: Automated method for lidar determination of cloud-base height and vertical extent. Applied optics, 31(10), pp.1488-1494., 1992.

Pelly, J.L. and Belcher, S.E.: A mixed-layer model of the well-mixed stratocumulus-topped boundary layer. Boundary-layer meteorology, 100, pp.171-187., 2001.

Poll, S., Shrestha, P. and Simmer, C.: Grid resolution dependency of land surface heterogeneity effects on boundary‐layer structure. Quarterly Journal of the Royal Meteorological Society, 148(742), pp.141-158., 2022.

Qian, Y., Guo, Z., Larson, V.E., Leung, L.R., Lin, W., Ma, P.L., Wan, H., Wang, H., Xiao, H., Xie, S. and Yang, B.: Region and cloud regime dependence of parametric sensitivity in E3SM atmosphere model. Climate Dynamics, pp.1-17., 2023.

Raju, V.G., Lakshmi, K.P., Jain, V.M., Kalidindi, A. and Padma, V.: August. Study the influence of normalization/transformation process on the accuracy of supervised classification. In 2020 Third International Conference on Smart Systems and Inventive Technology (ICSSIT) (pp. 729-735). IEEE., 2020.

Randles, C.A., Da Silva, A.M., Buchard, V., Colarco, P.R., Darmenov, A., Govindaraju, R., Smirnov, A., Holben, B., Ferrare, R., Hair, J. and Shinozuka, Y.: The MERRA-2 aerosol reanalysis, 1980 onward. Part I: System description and data assimilation evaluation. Journal of climate, 30(17), pp.6823-6850., 2017.

Rasp, S.: Coupled online learning as a way to tackle instabilities and biases in neural network parameterizations: general algorithms and Lorenz 96 case study (v1. 0). Geoscientific Model Development, 13(5), pp.2185-2196., 2020.

Rieck, M., Hohenegger, C. and van Heerwaarden, C.C.: The influence of land surface heterogeneities on cloud size development. Monthly Weather Review, 142(10), pp.3830-3846., 2014.

Ritsche, M.: ARM Surface Meteorology Systems Instrument Handbook. PNNL: Richland, WA, USA., 2011.

Romps, D.M.: Exact expression for the lifting condensation level. Journal of the Atmospheric Sciences, 74(12), pp.3891-3900., 2017.

Sakaguchi, K., Berg, L.K., Chen, J., Fast, J., Newsom, R., Tai, S.L., Yang, Z., Gustafson Jr, W.I., Gaudet, B.J., Huang, M. and Pekour, M.: Determining spatial scales of soil moisture—Cloud coupling pathways using semi‐idealized simulations. Journal of Geophysical Research: Atmospheres, 127(2), p.e2021JD035282., 2022.

Salimans, T., & Kingma, D. P.: Weight normalization: A simple reparameterization to accelerate training of deep neural networks. Advances in neural information processing systems, 29., 2016.

Shamekh, S., Lamb, K. D., Huang, Y., & Gentine, P.: Implicit learning of convective organization explains precipitation stochasticity. Proceedings of the National Academy of Sciences, 120(20), e2216158120., 2023.

Sisterson, D. L., Peppler, R. A., Cress, T. S., Lamb, P. J., & Turner, D. D.: The ARM Southern Great Plains (SGP) Site. Meteorological Monographs, 57(1), 6.1-6.14. https://doi.org/10.1175/AMSMONOGRAPHS-D-16-0004.1, 2016.

Song, H., Lin, W., Lin, Y., Wolf, A. B., Donner, L. J., Del Genio, A. D., ... & Liu, Y.: Evaluation of cloud fraction simulated by seven SCMs against the ARM observations at the SGP site. Journal of climate, 27(17), 6698-6719., 2014.

Stull, R.B.: An Introduction to Boundary Layer Meteorology. Dordrecht: Springer Netherlands, 1988.

Su, T.: Codes and Package of Deep Learning Driven Simulations of Boundary Layer Cloud over the US Southern Great Plains [Dataset]. Zenodo. https://doi.org/10.5281/zenodo.10685605, 2024.

Su, T., & Zhang, Y.: Deep-learning-derived planetary boundary layer height from conventional meteorological measurements. Atmospheric Chemistry and Physics, 24(11), 6477-6493., 2024.

Su, T., Li, Z. and Zheng, Y.: Cloud‐Surface Coupling Alters the Morning Transition From Stable to Unstable Boundary Layer. Geophysical Research Letters, 50(5), p.e2022GL102256., 2023.

Su, T., Li, Z., and Kahn, R.: A new method to retrieve the diurnal variability of planetary boundary layer height from lidar under different thermodynamic stability conditions. Remote Sens. Environ., 237, 111519., 2020.

Su, T., Li, Z., Zhang, Y., Zheng, Y., & Zhang, H.: Observation and reanalysis derived relationships between cloud and land surface fluxes across cumulus and stratiform coupling over the Southern Great Plains. Geophysical Research Letters, 51(8), e2023GL108090., 2024.

Su, T., Zheng, Y. and Li, Z.: Methodology to determine the coupling of continental clouds with surface from lidar and meteorological data. Atmos. Chem. Phys., 2022.

Tang, Q., Xie, S., Zhang, Y., Phillips, T. J., Santanello, J. A., Cook, D. R., Riihimaki, L. D., and Gaustad, K. L.: Heterogeneity in warm-season land-atmosphere coupling over the US Southern Great Plains, J. Geophys. Res.-Atmos., 123.: 7882, (2018)., 7867.

Tang, S., Xie, S., Zhang, M., Tang, Q., Zhang, Y., Klein, S. A., Cook, D. R., and Sullivan, R. C.: Differences in eddy‐correlation and energy‐balance surface turbulent heat flux measurements and their impacts on the large‐scale forcing fields at the ARM SGP site. J. Geophy. Res. Atmos., 124, 3301–3318, doi.org/10.1029/2018JD029689., 2019.

Tao, C., Zhang, Y., Tang, Q., Ma, H.Y., Ghate, V.P., Tang, S., Xie, S. and Santanello, J.A.: Land–Atmosphere coupling at the US Southern Great Plains: A comparison on local convective regimes between ARM observations, reanalysis, and climate model simulations. Journal of Hydrometeorology, 22(2), pp.463-481., 2021.

Tao, C., Zhang, Y., Tang, S., Tang, Q., Ma, H.Y., Xie, S. and Zhang, M.: Regional moisture budget and land‐atmosphere coupling over the US Southern Great Plains inferred from the ARM long‐term observations. Journal of Geophysical Research: Atmospheres, 124(17-18), pp.10091-10108., 2019.

Teixeira, J., and Hogan, T. F.: Boundary layer clouds in a global atmospheric model: simple cloud cover parameterizations. J. Climate, 15(11), 1261–1276., 2002.

Tian, J., Zhang, Y., Klein, S.A., Öktem, R. and Wang, L.: How does land cover and its heterogeneity length scales affect the formation of summertime shallow cumulus clouds in observations from the US Southern Great Plains?. Geophysical Research Letters, 49(7), p.e2021GL097070., 2022.

Tiedtke, M.: Representation of clouds in large-scale models. Monthly Weather Review, 121(11), 3040-3061., 1993.

Vassallo, D., Krishnamurthy, R., and Fernando, H. J. S.: Decreasing wind speed extrapolation error via domain-specific feature extraction and selection, Wind Energ. Sci., 5, 959–975, https://doi.org/10.: wes-5-959-2020, (2020)., 5194.

Wang, C., Platnick, S., Meyer, K., Zhang, Z. and Zhou, Y.: A machine-learning-based cloud detection and thermodynamic-phase classification algorithm using passive spectral observations. Atmospheric Measurement Techniques, 13(5), pp.2257-2277., 2020.

Wang, Y., Zheng, X., Dong, X., Xi, B. and Yung, Y.L.: Insights of warm-cloud biases in Community Atmospheric Model 5 and 6 from the single-column modeling framework and Aerosol and Cloud Experiments in the Eastern North Atlantic (ACE-ENA) observations. Atmospheric Chemistry and Physics, 23(15), pp.8591-8605., 2023.

Xiao, H., Berg, L.K. and Huang, M.: The impact of surface heterogeneities and land‐atmosphere interactions on shallow clouds over ARM SGP site. Journal of Advances in Modeling Earth Systems, 10(6), pp.1220-1244., 2018.

Xiao, H., Berg, L.K. and Huang, M.: The impact of surface heterogeneities and land‐atmosphere interactions on shallow clouds over ARM SGP site. Journal of Advances in Modeling Earth Systems, 10(6), pp.1220-1244., 2018.

Xie, S., McCoy, R. B., Klein, S. A., Cederwall, R. T., Wiscombe, W. J., Jensen, M. P., Johnson, K. L., Clothiaux, E. E., Gaustad, K. L., Long, C. N., and Mather, J. H.: Clouds and more: ARM climate modeling best estimate data: a new data product for climate studies. Bull. Amer. Meteorol. Soc., 91(1), 13–20., 2010.

Yang, Y., Zheng, X., Gao, Z., Wang, H., Wang, T., Li, Y., Lau, G.N. and Yim, S.H.:

Long‑term trends of persistent synoptic circulation events in planetary boundary layer and their relationships with haze pollution in winter half year over eastern China. Journal of Geophysical Research: Atmospheres, 123(19), pp.10-991., 2018.

Yeo, H., Kim, M.H., Son, S.W., Jeong, J.H., Yoon, J.H., Kim, B.M. and Kim, S.W.: Arctic cloud properties and associated radiative effects in the three newer reanalysis datasets (ERA5, MERRA-2, JRA-55): Discrepancies and possible causes. Atmospheric Research, 270, p.106080., 2022.

Zhang, L., Dong, X., Kennedy, A., Xi, B. and Li, Z.: Evaluation of NASA GISS post-CMIP5 single column model simulated clouds and precipitation using ARM Southern Great Plains observations. Advances in Atmospheric Sciences, 34, pp.306-320., 2017.

Zhang, T., Lin, W., Vogelmann, A.M., Zhang, M., Xie, S., Qin, Y. and Golaz, J.C.: Improving convection trigger functions in deep convective parameterization schemes using machine learning. Journal of Advances in Modeling Earth Systems, 13(5), p.e2020MS002365., 2021.

Zhang, Y. and Klein, S.A.: Mechanisms affecting the transition from shallow to deep convection over land: Inferences from observations of the diurnal cycle collected at the ARM Southern Great Plains site. Journal of the Atmospheric Sciences, 67(9), pp.2943-2959., 2010.

Zhang, Y. and Klein, S.A.: Factors controlling the vertical extent of fair-weather shallow cumulus clouds over land: Investigation of diurnal-cycle observations collected at the ARM Southern Great Plains site. Journal of the Atmospheric Sciences, 70(4), pp.1297-1315., 2013.

Zhang, Y., B. Stevens, B. Medeiros, and M. Ghil.: Low-Cloud Fraction, Lower-Tropospheric Stability, and Large-Scale Divergence. J. Climate, 22, 4827–4844, https://doi.org/10.1175/2009JCLI2891.1., 2009.

Zhang, Y., Klein, S.A., Fan, J., Chandra, A.S., Kollias, P., Xie, S. and Tang, S.: Large-eddy simulation of shallow cumulus over land: A composite case based on ARM long-term observations at its Southern Great Plains site. Journal of the Atmospheric Sciences, 74(10), pp.3229-3251., 2017.

Zhang, Y., Stevens, B. and Ghil, M.: On the diurnal cycle and susceptibility to aerosol concentration in a stratocumulus-topped mixed layer. Q.J.R. Meteorol. Soc., 131: 1567-1583. https://doi.org/10.1256/qj.04.103, 2005.

Zheng, X., Tao, C., Zhang, C., Xie, S., Zhang, Y., Xi, B. and Dong, X.: Assessment of CMIP5 and CMIP6 AMIP simulated clouds and surface shortwave radiation using ARM observations over different climate regions. Journal of Climate, 36(24), pp.8475-8495., 2023.

TABLE LIST:

Table 1: Detailed descriptions of input and output variables used in the deep learning models for predicting boundary layer clouds (BLCs). The table includes the variable names, descriptions, and data sources. For the input parameters, surface meteorology and fluxes are taken from the current and previous hours, while morning profiles comprises 46 values spanning from 0-8 km at 06 LT. Note that the output data is derived from ARSCL (Active Remote Sensing of Clouds). The three outputs correspond to the trigger module, cloud-base module, and fraction-thickness module, respectively.

Variable	Description	Data Source
Input		
Month	Range from 1-12	Time Record
LT	Local Time	Time Record
PS	Pressure at surface level (2m)	Surface Meteorology Station
RH	Relative Humidity at 2m	Surface Meteorology Station
U	Zonal wind at 2m	Surface Meteorology Station
V	Meridional wind at 2m	Surface Meteorology Station
T	Temperature at 2m	Surface Meteorology Station
LCL	Lifted Condensation Level	Derived from T, RH, PS
SH	Sensible Heat	Energy Balance Bowen Ratio
LH	Latent Heat	Energy Balance Bowen Ratio
RH Profile	Morning RH profiles	Radiosonde
U Profile	Morning U wind profiles	Radiosonde
V Profile	Morning V wind profiles	Radiosonde
θ Profile	Morning potential temperature profiles	Radiosonde
BLH_{SH}	PBLH derived from sensible heat	Derived from θ Profile and SH
BLH_{Parcel}	PBLH derived from parcel method	Derived from θ Profile and T
Output		
Trigger	Cloud occurrence	ARSCL
Position	Cloud-base height	ARSCL
Fraction Profiles	Cloud fraction and thickness	ARSCL

Table 2: Classification Performance of the Deep Learning Model for Boundary Layer Clouds (BLC) Trigger. This table present the performance metrics of the deep learning model during both the trained and untrained periods. It lists the number of samples and corresponding percentages for true negatives (TN), false positives (FP), false negatives (FN), and true positives (TP). The overall accuracy for each period is also provided, indicating the model's overall effectiveness in predicting the presence of boundary layer clouds.

Performance Metrics	Trained Period (1998-2016)		Untrained Period (2017-2020)	
	Sample #	Percentage (%)	Sample #	Percentage (%)
TN	9773	71.1747142	5416	71.8016704
FP	393	2.8621368	393	5.2101286
FN	670	4.8794698	424	5.6211057
TP	2895	21.0836793	1310	17.3670953
Overall Accuracy	N.A.	92.2583934	N.A.	89.1687657
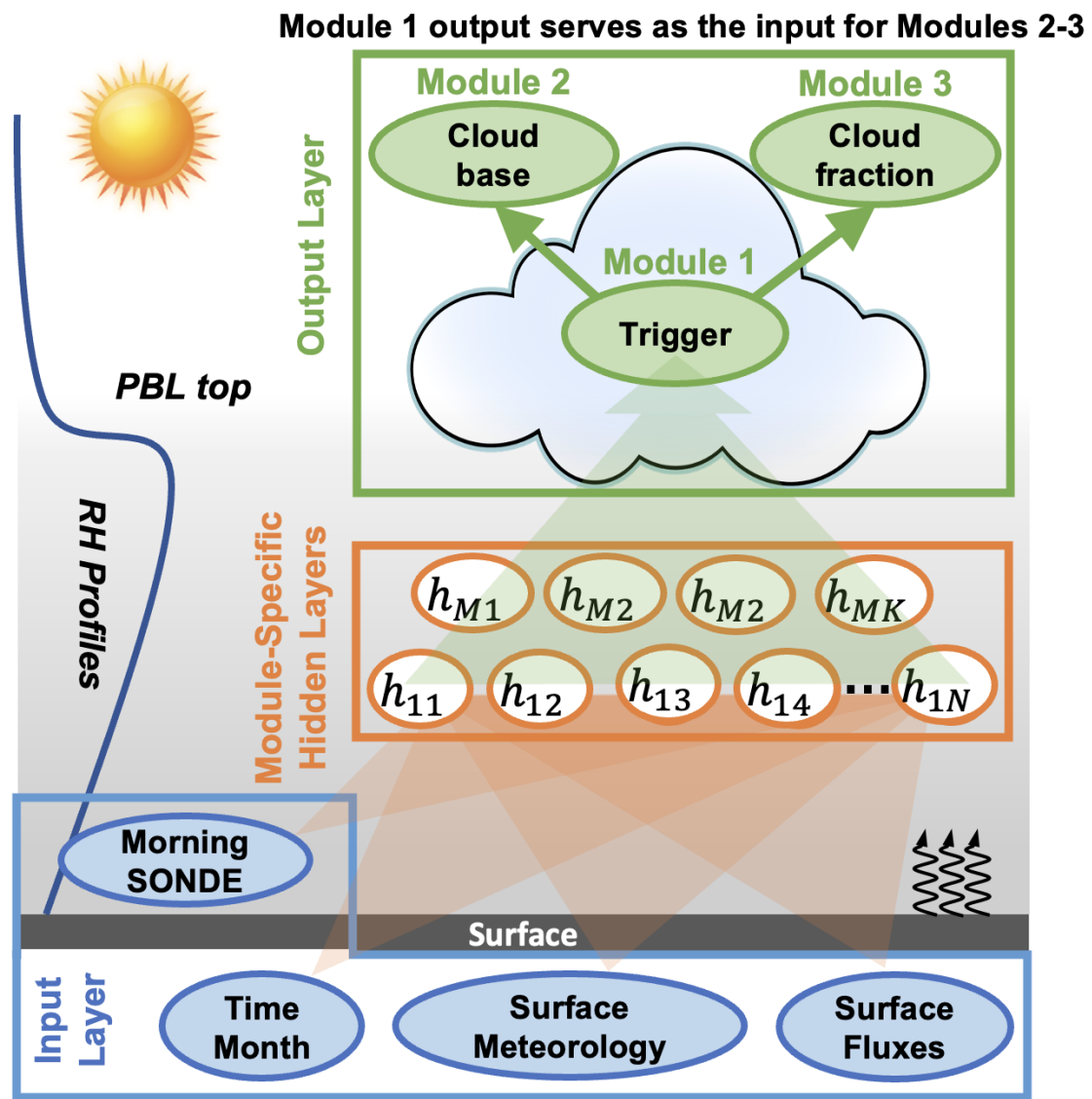
Figures

Figure 1: Conceptual diagram of the deep learning framework for simulating boundary layer cloud (BLC) characteristics over the US Southern Great Plains. Inputs for the deep neural networks (DNN) include morning ~~meteorological profiles from~~ radiosonde (SONDE~~) profiles,~~)~~,~~ time indicators~~,~~ (i.e., local time and month), and surface conditions such as fluxes (curved black arrows) and meteorological data. The relevance of relative humidity (RH) profiles and the planetary boundary layer (PBL) top is emphasized due to their critical role in ~~boundary layer~~BLCs development. These variables are processed through multiple layers of hidden neurons ($h_{11}$$h_{11}$ to h_{MK}), ~~each with neuron bias adjustments to optimize the network's predictive capability.~~h_{MK}). Both input and output parameters are hourly, except for the morning SONDE. Separate DNN ~~models~~modules are constructed for each task: Module 1 handles the initiation (trigger) of ~~boundary layer clouds (~~BLC~~), their vertical positioning, and~~; Module 2 estimates the cloud base; and Module 3 estimates cloud fraction ~~across ten atmospheric layers~~and thickness. Together, these models synergize to predict the presence, altitude, and stratification of BLC.
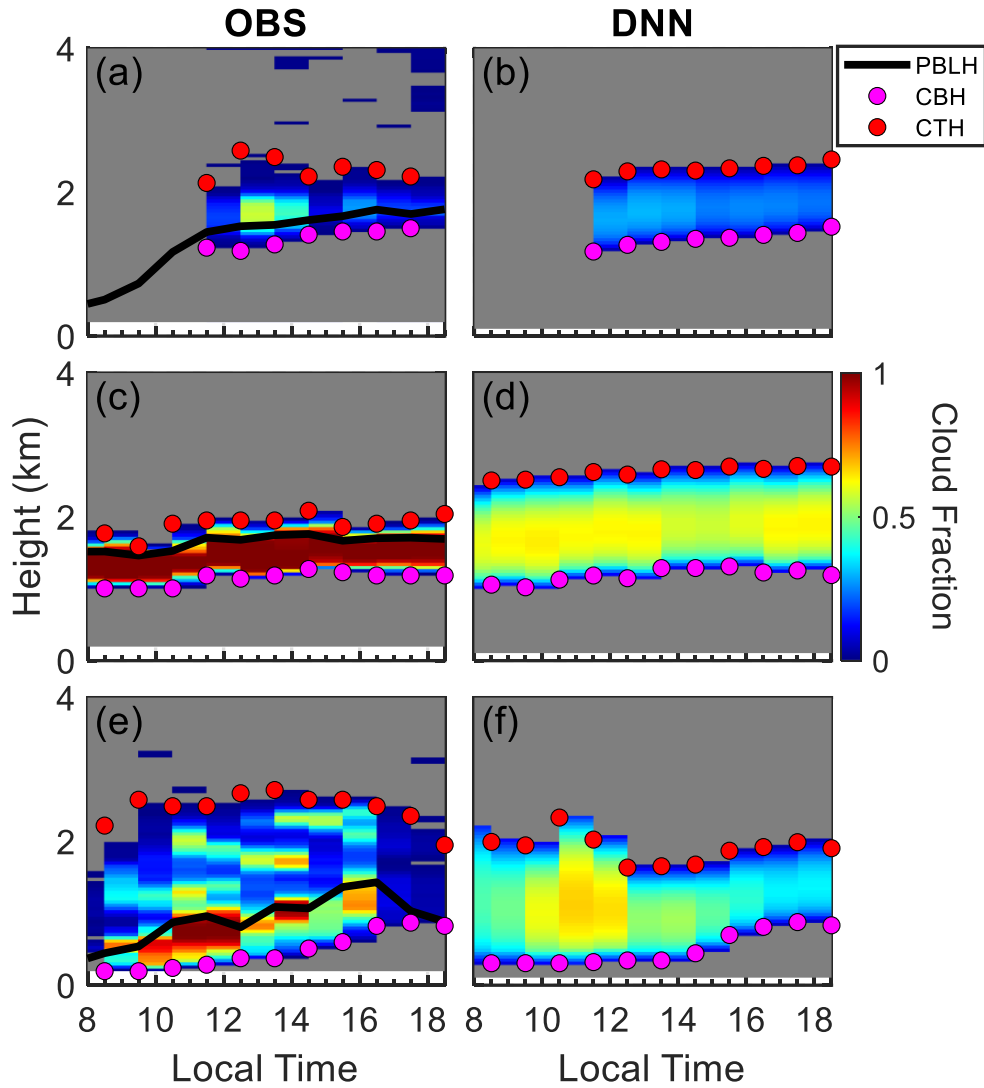
1283

Figure 2: Examples of diurnal cloud fraction profiles for cumulus (a, b), stratiform (c, d), and complex cloud structures (e, f) over the US Southern Great Plains. Observed data (OBS) are shown alongside deep learning neural network (DNN) simulations. Black lines represent the observed PBL height (PBLH), with cloud base (CBH) and cloud top heights (CTH) marked by pink and red dots, respectively. The color gradient indicates the cloud fraction.
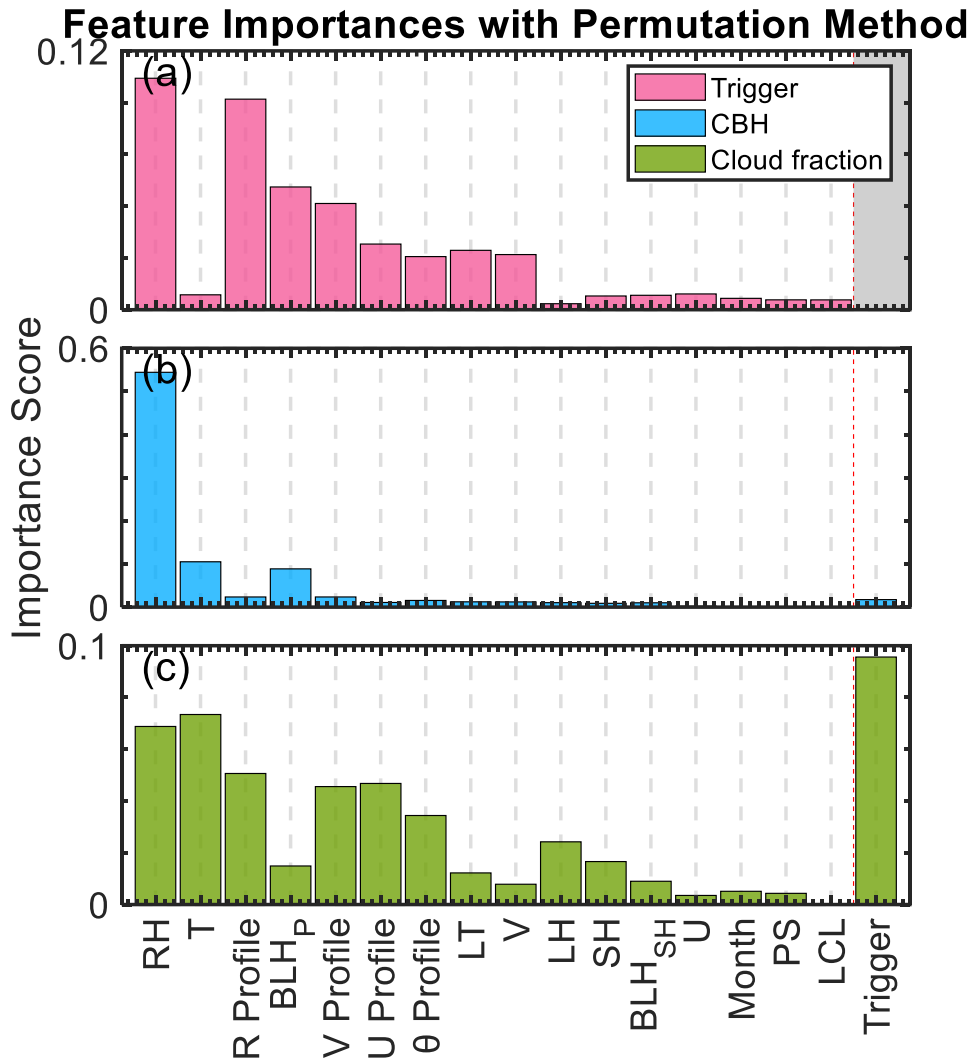
Figure 3. Feature importance scores for predicting cloud ~~trigger~~occurrence (a), cloud base height (CBH) (b), and cloud fraction (c) in the deep learning simulations of BLCs. Each panel presents the relative contribution of input features, includes month, local time (LT), surface pressure (PS), relative humidity (RH), zonal (U) and meridional (V) wind components, temperature (T), lifting condensation level (LCL), boundary layer height derived from sensible heat (BLH$_{SH}$) and parcel methods (BLH$_{Parcel}$), sensible heat (SH), latent heat (LH), and morning profiles of relative humidity (R Profile), U wind (U Profile), V wind (V Profile), and potential temperature (θ Profile). These factors are ranked based on their overall importance. The importance scores are calculated with permutation method and quantify the relative contribution of each feature to the model's predictive accuracy.
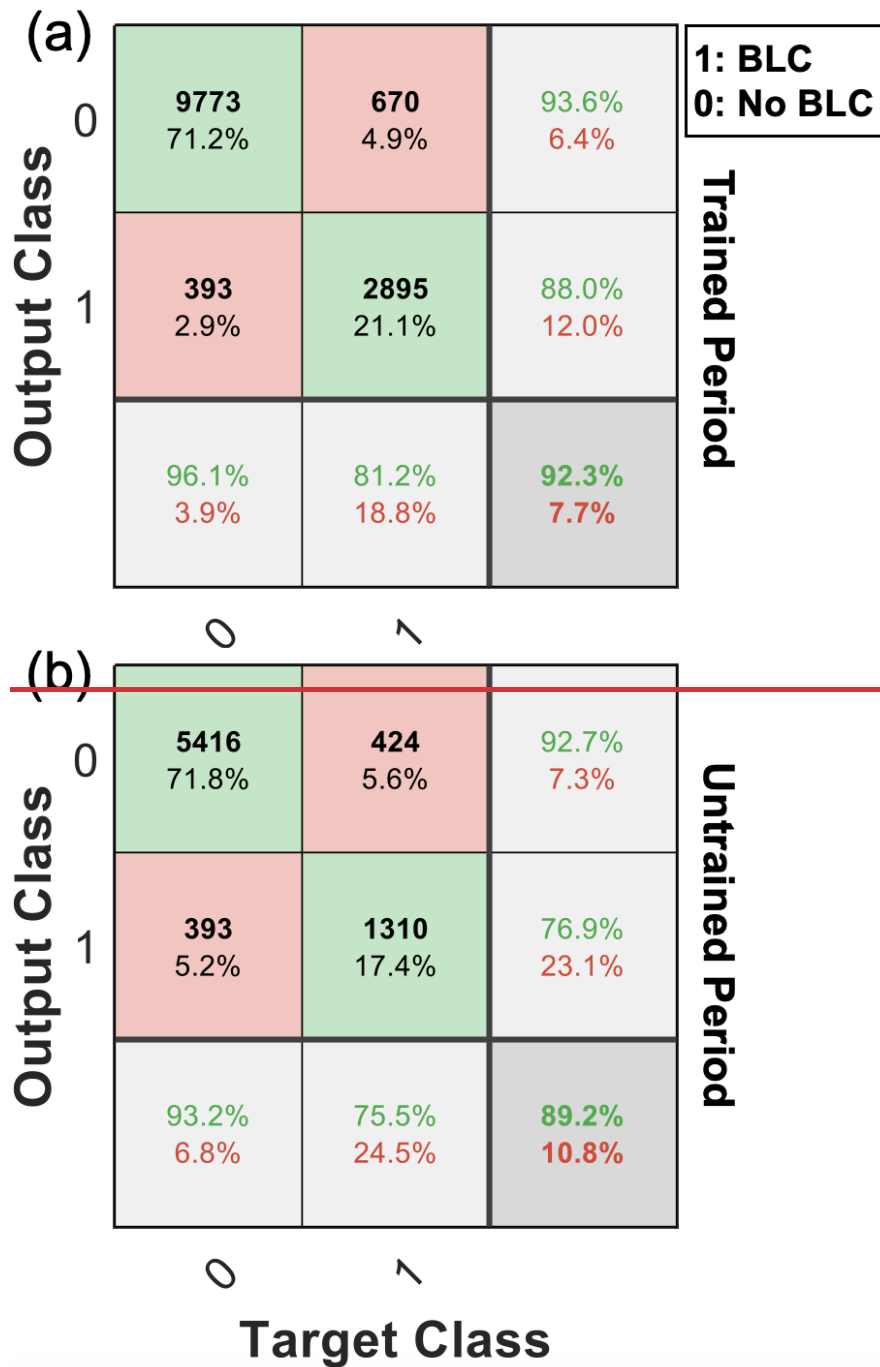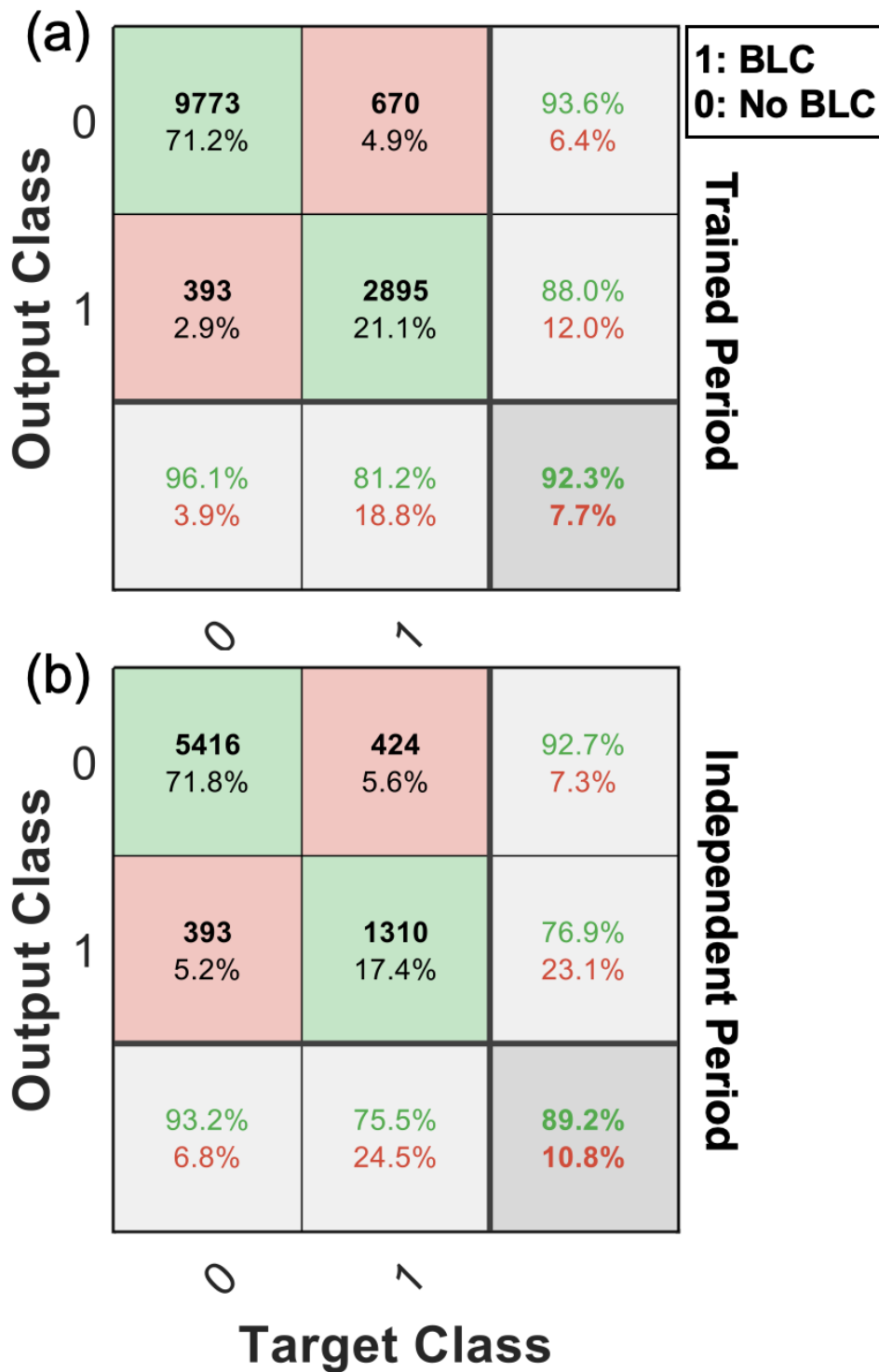
Figure 4: Confusion matrices ~~representing~~on the classification performance of the deep learning model ~~for~~in predicting the ~~presence~~occurrence of boundary layer clouds (BLCs) during the trained period (1998-2016) in panel (a), and the ~~untrained~~independent period (2017-2020) in panel (b). ~~For~~The matrices in the trained period~~, we use~~ are calculated using the 30% dataset for the validation. The matrices in the black color display the counts and percentages of true positive (TP), false positive (FP), true negative (TN), and false negative (FN) predictions. The overall accuracy, precision, and recall~~, and F1~~ scores for each class are also included, demonstrating the

1312   model's ability in identifying BLC occurrence.
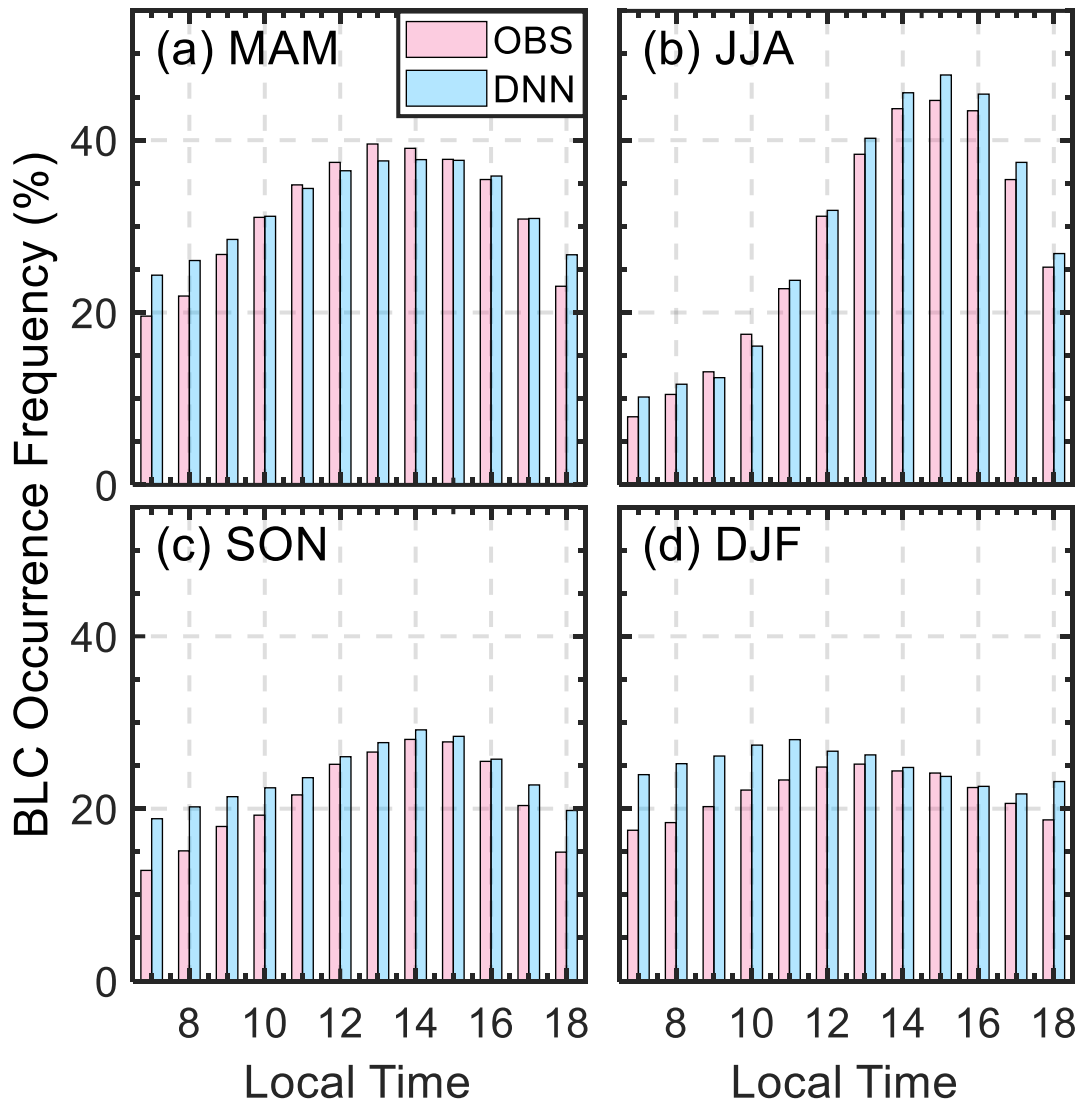
1313

1314 **Figure 5.** Bar graph ~~comparing~~comparison on the occurrence frequency of boundary
1315 layer ~~cloud~~clouds (BLC) ~~occurrence as~~between the observed (OBS, red) and ~~as~~the
1316 predicted by the deep learning neural network (DNN, blue) across different local times
1317 of the day, segmented by seasons: (a) MAM (Spring), (b) JJA (Summer), (c) SON (Fall),
1318 and (d) DJF (Winter). ~~The bars present the diurnal pattern of BLC development.~~

1319

1320

1321
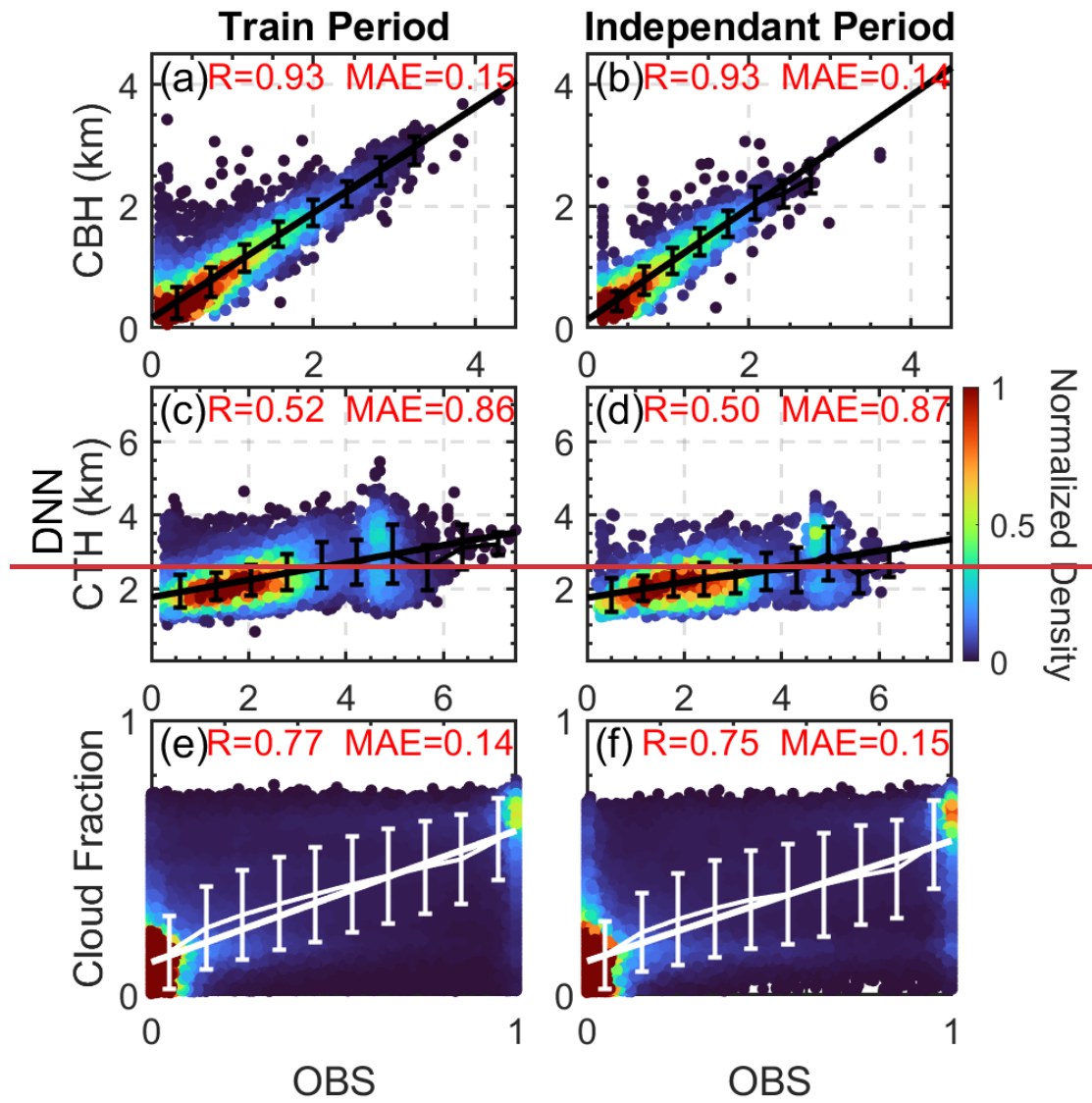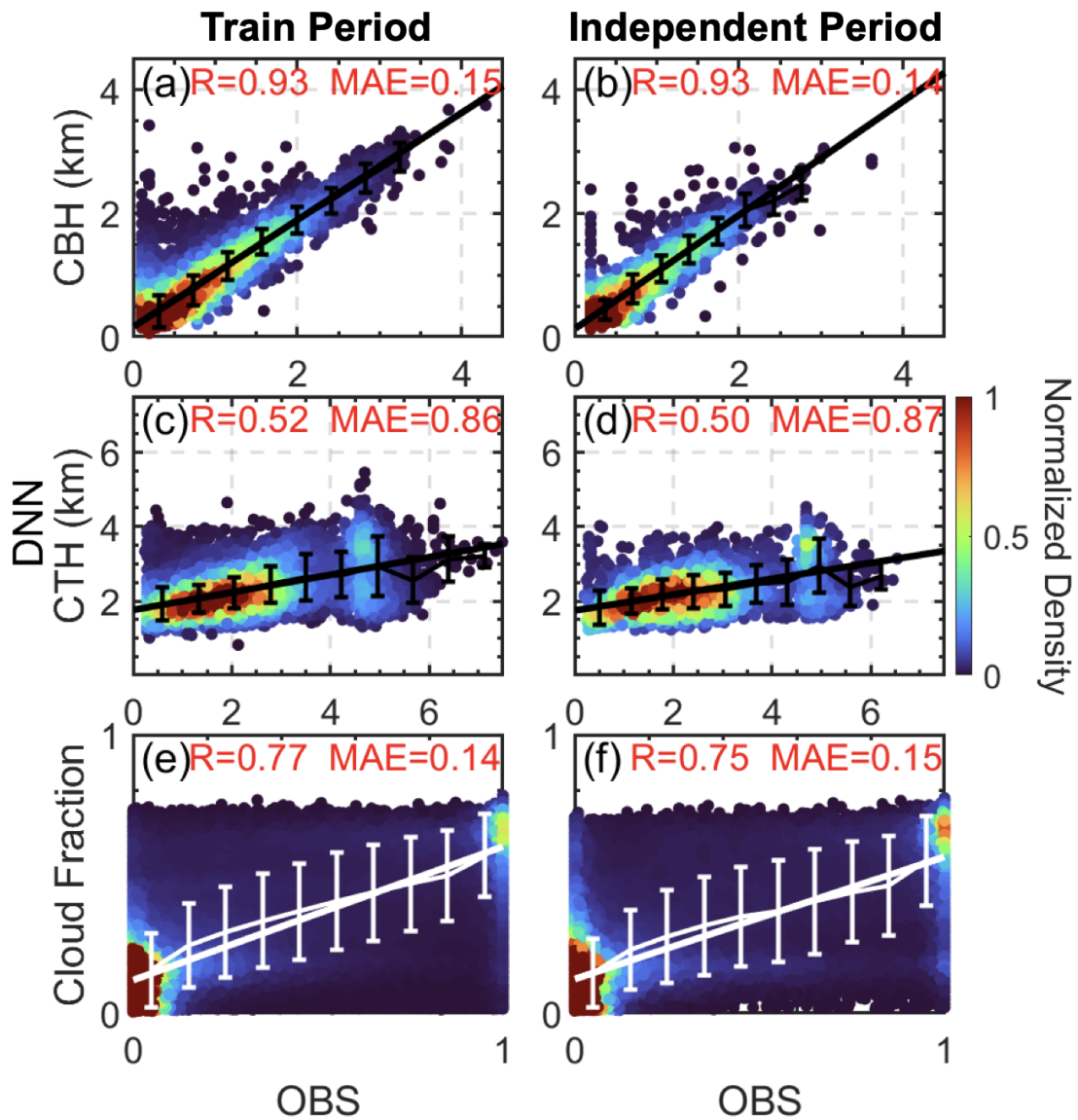
Figure 6. Scatter density ~~plots comparing~~ comparison between the observed (OBS) and the predicted values by the deep learning neural network (DNN) ~~predicted values~~ for cloud base height (CBH), cloud top height (CTH), and cloud fraction during the ~~train~~trained period (a, c, e) and an independent period (b, d, f). Note that the BLC is segmented into ten layers, yielding ten separate cloud fraction values per BLC instance for analysis. The correlation coefficient (R) and mean absolute error (MAE) are indicated for each comparison. The color scale represents the normalized density of data points. The solid lines and error bars denoting the linear regression and standard deviations in each bar.
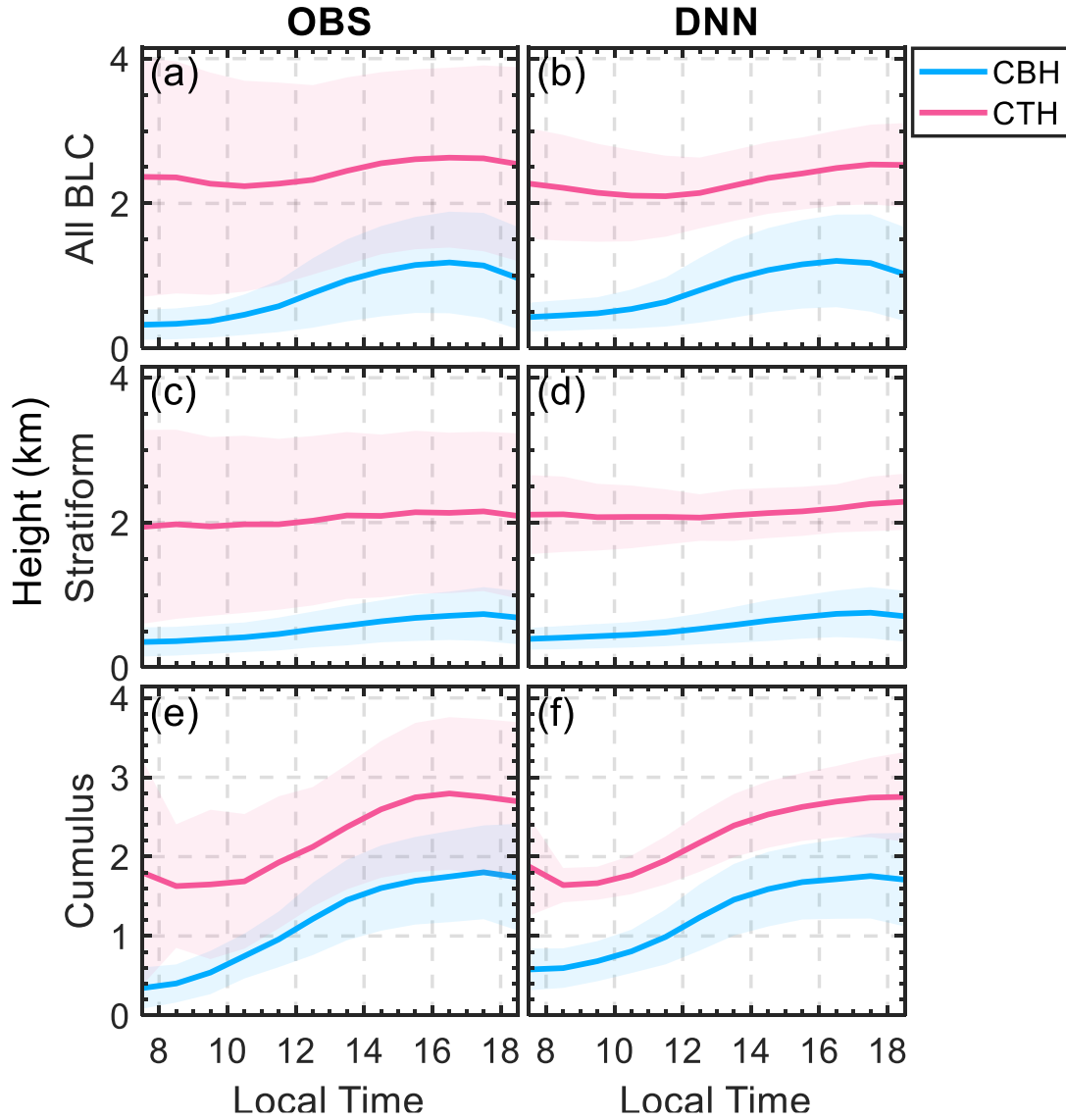
Figure 7. Diurnal profiles of cloud base height (CBH) and cloud top height (CTH) as determined by the observations (OBS) and deep learning simulations for all BLC (a-b), stratiform clouds (c-d), and cumulus (e-f). The shaded areas represent the variability (one standard deviation) around the mean heights.
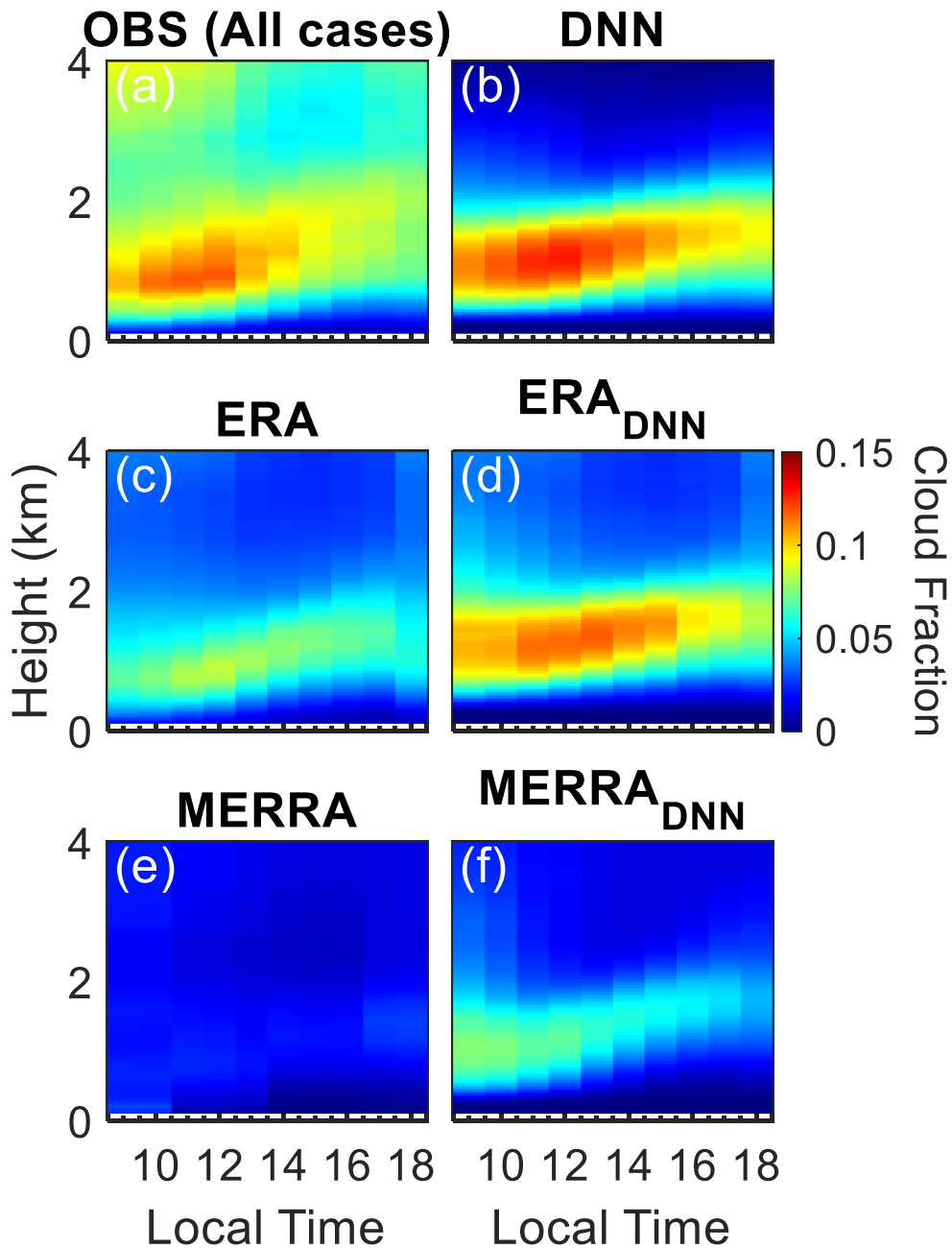
Figure 8. ~~Cloud~~Color shaded areas demonstrate the diurnal variation in cloud fraction for all cases as observed and simulated. Panel (a) shows the observed cloud fraction (OBS), while panel (b) illustrates the cloud fraction simulated by the deep learning neural networks (DNN~~).)~~ using ARM observational data as inputs. (c, e): cloud fractions direcly extracted from ERA and MERRA reanalysis datasets, respectively. (d, f): the cloud fractions ~~after the application of~~simulated by the DNN model ~~to~~using ERA (ERA$_{DNN}$) and MERRA (MERRA$_{DNN}$) data as inputs.
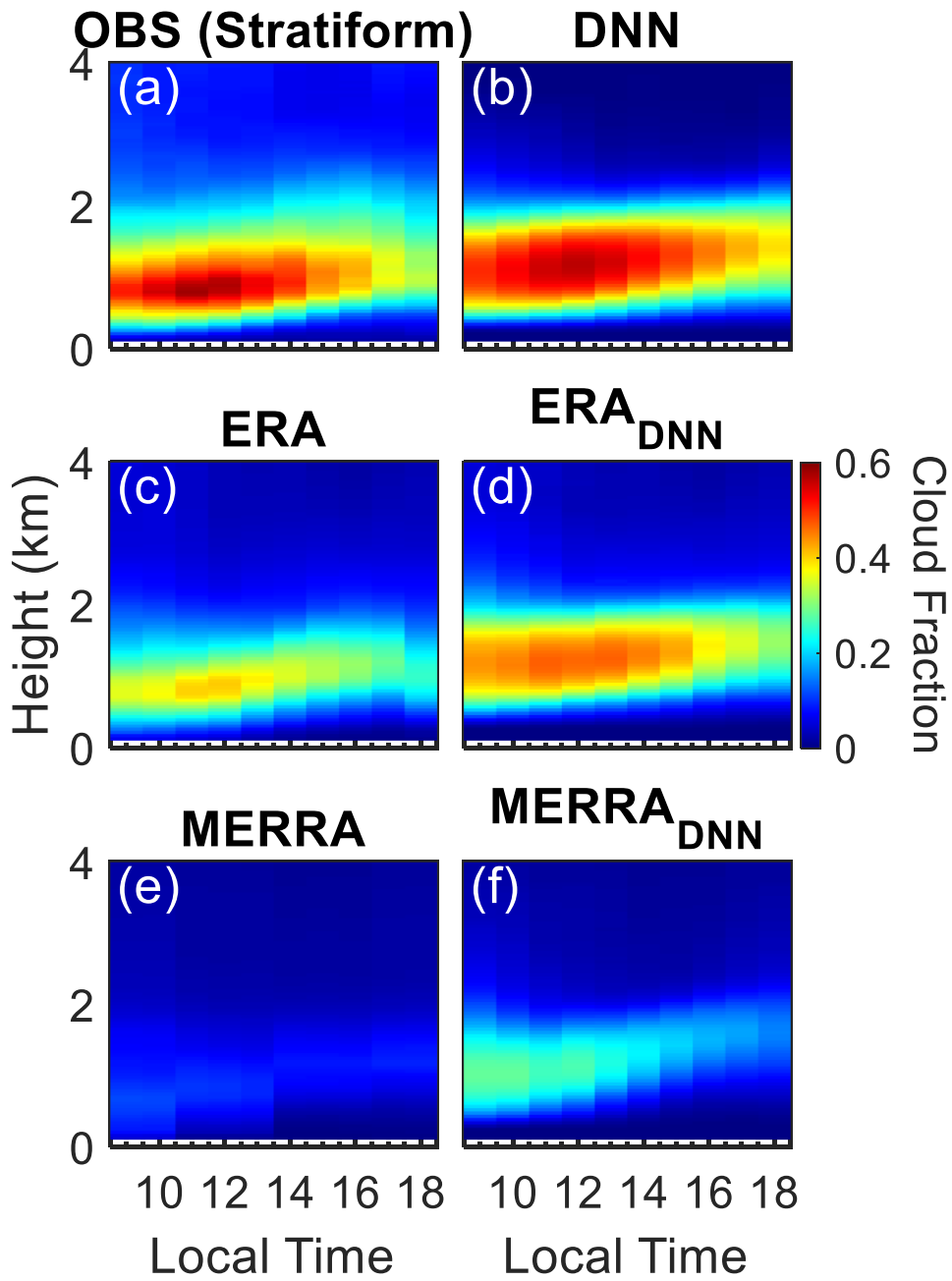
1348

1349 **Figure 9.** Same to Figure 8, but for stratiform clouds.
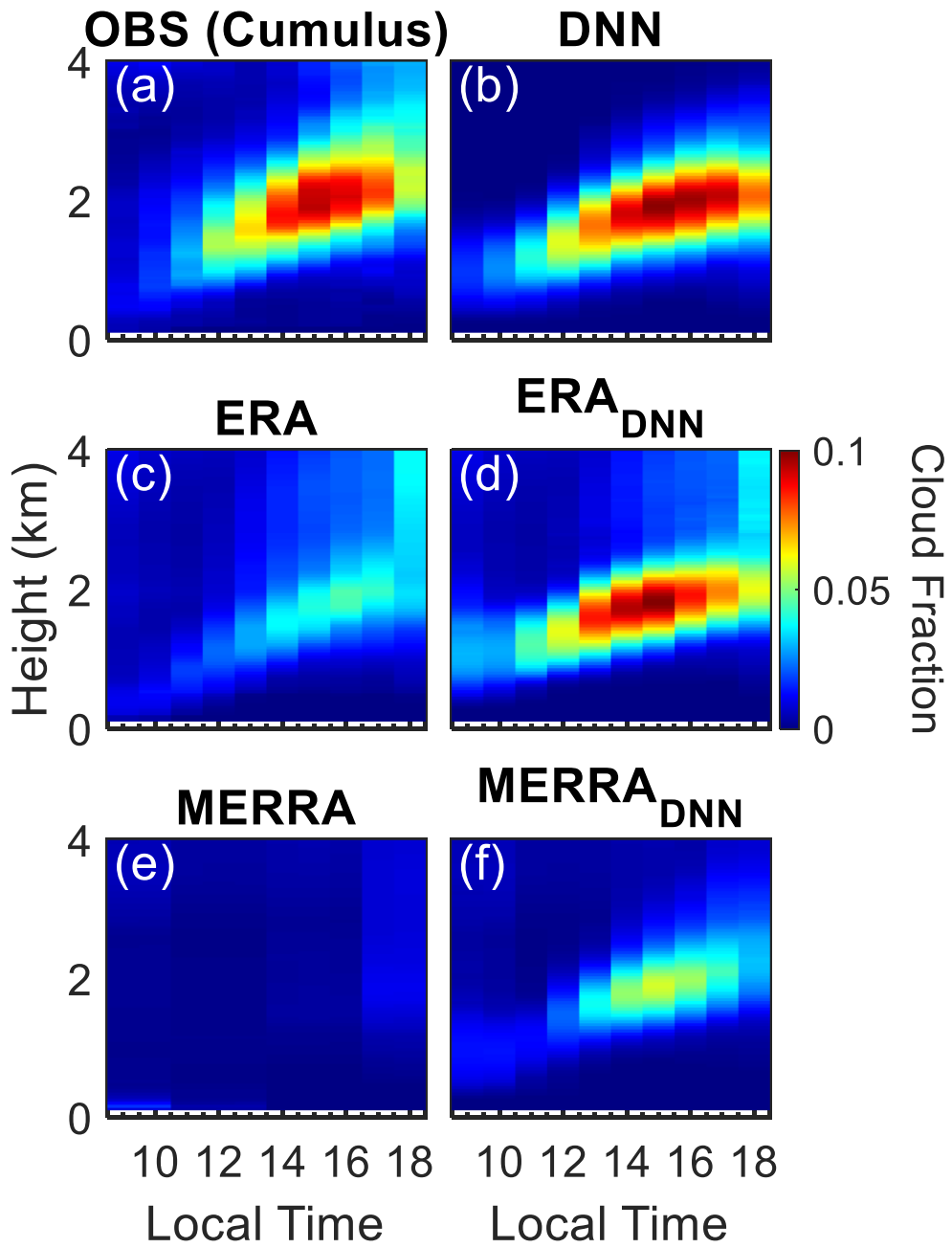
1350

Figure 10. Same to Figure 8, but for cumulus.

1352
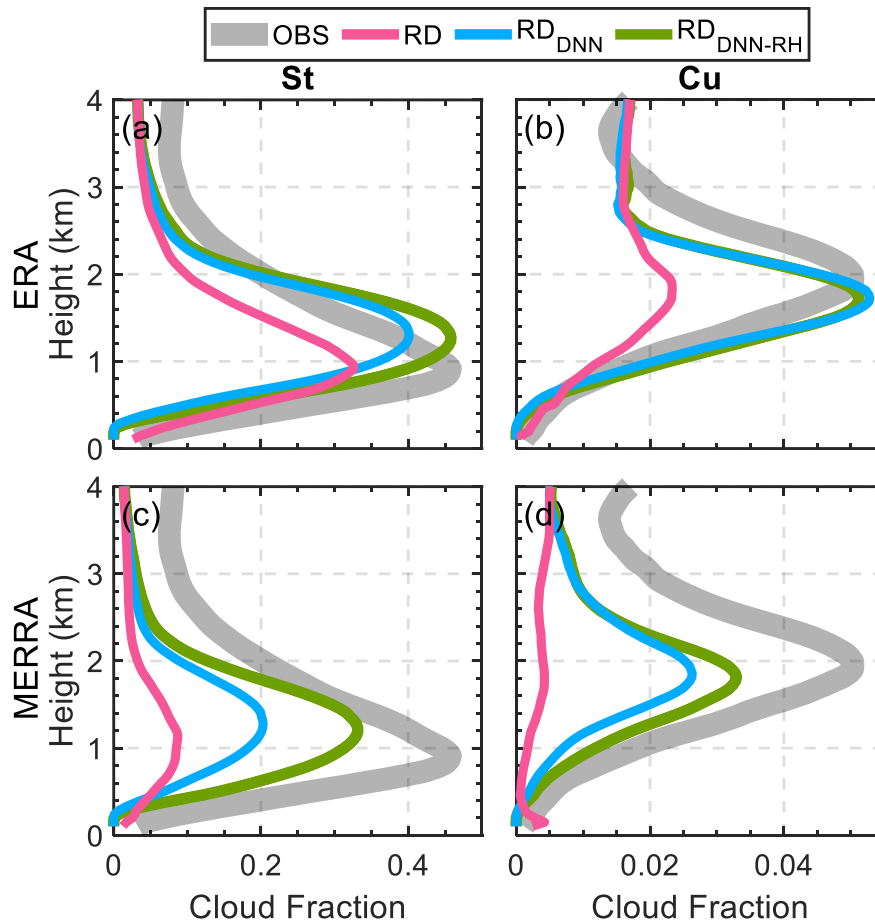
Figure 11: Vertical profiles of cloud fraction for stratiform (St) and cumulus (Cu) scenarios over the US Southern Great Plains. Panels (a) and (b) display ERA reanalysis data comparisons, while panels (c) and (d) show MERRA reanalysis data comparisons. The observed cloud fractions (OBS) are represented by the shaded grey area, illustrating the averaged cloud coverage recorded by field observations. The original reanalysis data (RD) is indicated in pink, indicating the baseline cloud fraction profiles as simulated by the reanalysis. The RD$_{DNN}$ profiles in blue depict the new simulation results after applying the DNN models to the reanalysis data for boundary layer cloud (BLC) simulation. The RD$_{DNN-RH}$ profiles in green show the simulation results when the surface relative humidity (RH) from the reanalysis data is replaced with observed values, indicating the impact of accurate surface moisture representation on cloud fraction simulations.
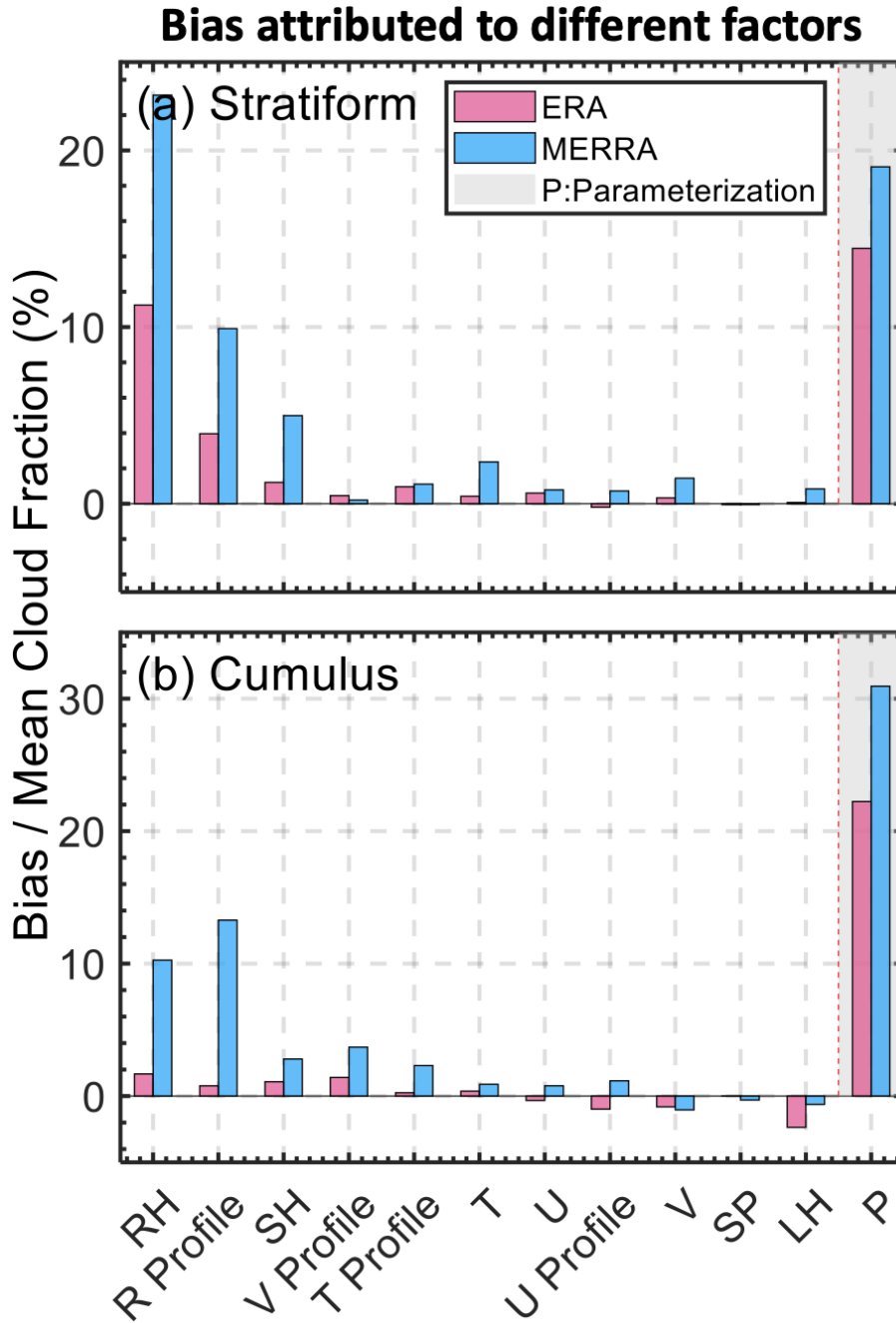
Figure 12: Attribution of bias between observed and reanalysis on cloud fractions to various meteorological factors and parameterization schemes for stratiform (a) and cumulus (b) cloud scenarios. The bars represent the normalized bias (bias divide mean cloud fraction) contributed by each factor: relative humidity profile (RH), meridional wind profile (V Profile), temperature profile (T Profile), zonal wind profile (U Profile), surface pressure (SP), latent heat flux (LH), and parameterization (P). All profiles took on morning (06:00 LT). Light blue bars indicate biases identified in the ERA reanalysis dataset, while pink bars represent biases in the MERRA reanalysis dataset. The dashed red line marked 'P' denotes biases attributed specifically to the parameterization within the reanalysis models. This analysis uses the DNN to discern the impact of each factor (ranked from highest to lowest) on the discrepancy in cloud fraction estimates between

1379   observations and reanalysis models.